Palacký University Olomouc
Faculty of Science
Department of Experimental Physics

DIPLOMA THESIS

Study of products of proton-proton collisions in forward region of ATLAS detector

Author: Josef Pácalt
Course of study: Applied physics
Form of study: Full time
Thesis supervisor: Mgr. Libor Nožka, Ph.D.

2014

I declare, that I worked on this diploma thesis independently under supervising Mgr. Libor Nožka, Ph.D using only sources listed in the list of sources and I would like to thank to my consultant Mgr. Petr Hamal and my supervisor for their patience, time and advices.

In Olomouc ……. ...…….....

Bibliografická identifikace:

Jméno a příjmení autora	Josef Pácalt
Název práce	Studium produktů proton-protonových srážek v dopředné části detektoru ATLAS
Typ práce	Magisterská
Pracoviště	Katedra experimentální fyziky
Vedoucí práce	Mgr. Libor Nožka, Ph.D.
Rok obhajoby práce	2014
Abstrakt	Práce uvádí popis LHC v CERNu a projekty na něm se zaměřením na ALFA detektor, analýzu rekonstrukční účinnosti pro data na optice jednoho kilometru a očekávané spektrum Mandelstamovy proměnné *t*, určené několika metodami.
Klíčová slova	CERN, LHC, ALFA, rekonstrukční účinnost, Mandelstamovy proměnné, ROOT
Počet stran	60
Počet příloh	1
Jazyk	Anglický

Bibliographical identification:

Author's first name and surname	Josef Pácalt
Title	Study of products of proton-proton collisions in forward region of ATLAS detector
Type of thesis	Master
Department	Department of Experimental Physics
Supervisor	Mgr. Libor Nožka, Ph.D.
The year of presentation	2014
Abstract	Work presents description of Large Hadron Collider in CERN and projects there, focusing on ALFA detector, reconstruction efficiency analysis for data on one kilometer optics and expected spectrum of Mandelstam variable *t* calculated by several methods.
Keywords	CERN, LHC, ALFA, reconstruction efficiency, Mandelstam variables, ROOT
Number of pages	60
Number of appendices	1
Language	English

Table of contents

Introduction

Objective of this work is to describe principles of reconstruction analysis and reconstruction of Mandelstam variable in ALFA detector and preliminary analysis on raw data with the help of CERN software.

Particle physics domain is important for understanding principles of early universe and for Standard Model theory. There are two main sources of data in particle physics, by observation of cosmological radiation and of processes by study by means of colliders with high energy particles. Discovery of Higgs boson and confirmation of prediction of Standard model is one of the latest successes on this field of physics. Peter Higgs obtained a Nobel Praise in the year 2013 for his prediction of Higgs boson.

This work deals with data from run 213268 gathered in CERN Large Hadron Collider from proton-proton collisions gathered 24-25th October 2012. The analysis presented in this work is one of the first made on these data. A lot of work is needed to be done, however, to fully understand this run.

This work consists of seven chapters. The first chapter is dedicated for short description of the Large Hadron Collider and ATLAS detectors. The second chapter is devoted to describe mechanism of Mandelstam variables. Next chapter illustrates methods used for calculating Mandelstam variable *t*. In the fourth chapter, theoretical description is presented of reconstruction efficiency and principle of calculation. The fifth chapter describes experimental setup used for gathering data. The sixth chapter is devoted to present results of analysis of reconstruction efficiency. In the last chapter, results are shown for reconstruction of Mandelstam variable *t*.

I would like to thank supervisor Mgr. Libor Nožka, PhD. and my consultant Mgr. Petr Hamal for their time, patience and time spent on this work.

1. Large Hadron Collider (LHC), ATLAS experiment and ALFA detectors

1.1 Description of LHC

The Large Hadron Collider is project running under European Organization for Nuclear Research also known as CERN. Nowadays, LHC is the largest collider in the world; build in years 1998-2008. The purpose of LHC is better understanding of particle physics, high-energy physics and standard model, confirmation or disproving the predicted particles by super symmetric theories. Furthermore we are close to explanation how the Big Bang happened by better understanding of this topic. Confirmation of standard model by founding the Higgs boson in year 2013 was one of the most expected outcomes of this project.

LHC is a circular tunnel buried beneath French-Swiss border 50 to 175 m underground near Geneva. The circumference of LHC is 26659 m and there are two beams of particles circulating around. Those two beams travel around the tunnel in two separate pipes in opposite directions and there has to be ultrahigh vacuum inside the pipes to prevent collisions with molecules of the gas. The beam consists either from protons or ions. The magnetic system used in the tunnel is very extensive. There are used two types of magnets, 1232 dipole magnets which bend the trajectory of particles and 392 quadrupole magnets used for the beam focusing. Those magnets are superconducting electromagnets which have to be cooled by liquid helium to the temperature −271.3°C. LHC have four preaccelerators which are linear accelerators for protons and lead, Proton Synchrotron Booster, Proton Synchrotron (PS) and Super Proton Synchrotron (SPS). [1, 2, 3]

1.2 Experiments on LHC

There are seven experiments running on Large Hadron Collider. Those experiments are ATLAS, CMS, LHCb, ALICE, TOTEM, LHCf and MoEDAL. ATLAS is abbreviation of A Torroidal LHC Apparatus, CMS is abbreviation of Compact Muon Solenoid, LHCb is shortcut for Large Hadron Collider-beauty, ALICE stands for of A Large Ion Collider Experiment, TOTEM is abbreviation of Total Elastic and diffractive cross section Measurement, LHCf is shortcut for Large Hadron Collider-forward and finally MoEDAL

means of Monopole and Exotics Detector At the LHC. Locations of large experiments and scheme of LHC is shown at Fig. 1. [2, 3]

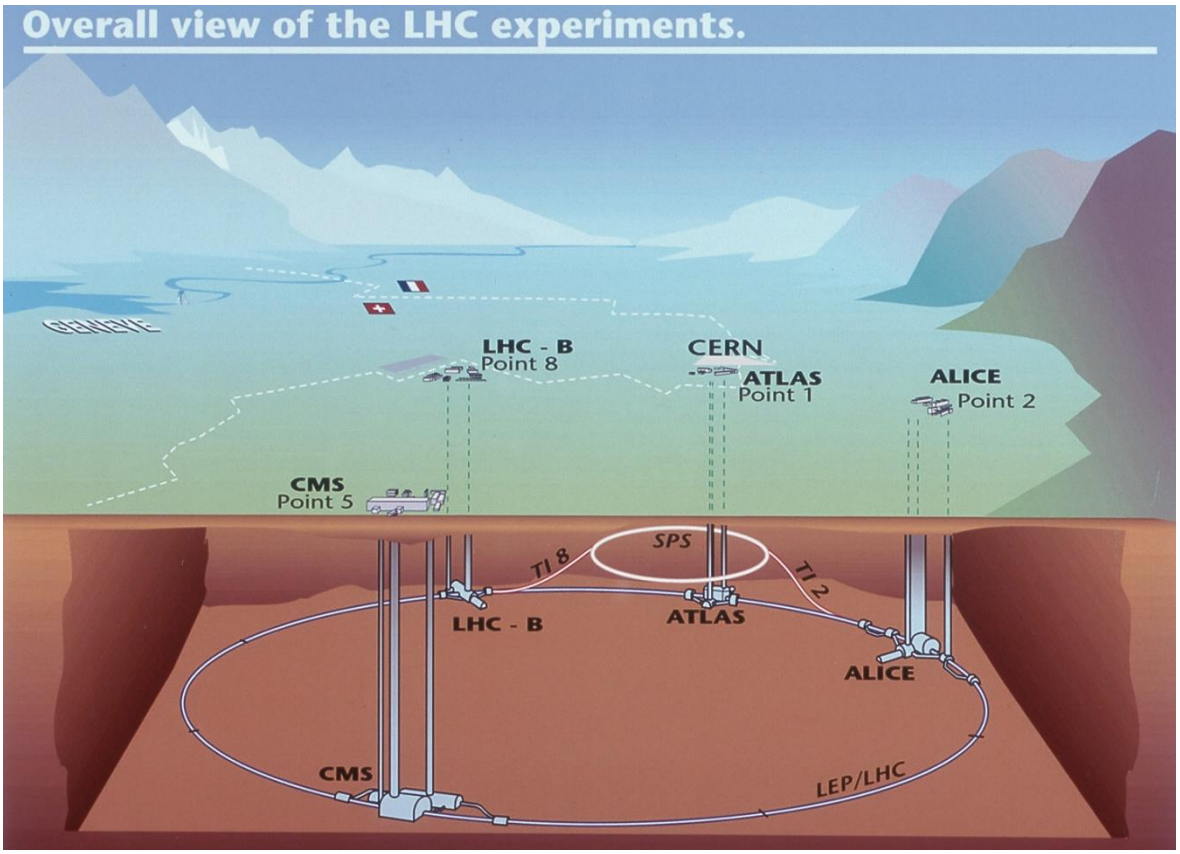

Fig. 1: The LHC layout and positions of the main experiments. (This figure is from[4])

1.3 ATLAS detector

As it was mentioned above, ATLAS is abbreviation of A Torroidal LHC Apparatus. ATLAS experiment has several detectors, main ATLAS detector and forward region ATLAS detectors.

The main ATLAS detector is constructed to cover almost entire solid angle. Detector has six layers for detecting as many information, as possible. The Pixel Detector is the first layer from interaction point, followed by Semi-Conductor Tracker (SCT) in the second layer and Transition Radiation Tracker (TRT) in the third layer. All three layers are designed for detection particle trajectory. Electromagnetic Calorimeter (EC) in the fourth layer and Hadron Calorimeter in the fifth layer are used to measure the energy of particles and can be found outside of solenoid magnet of the ATLAS. The last layer is formed by

Muon Spectrometer designed to measure momentum of muons. Main ATLAS detector is 46 m long and has 25 m in diameter; see Fig. 2 for detailed view. [5]

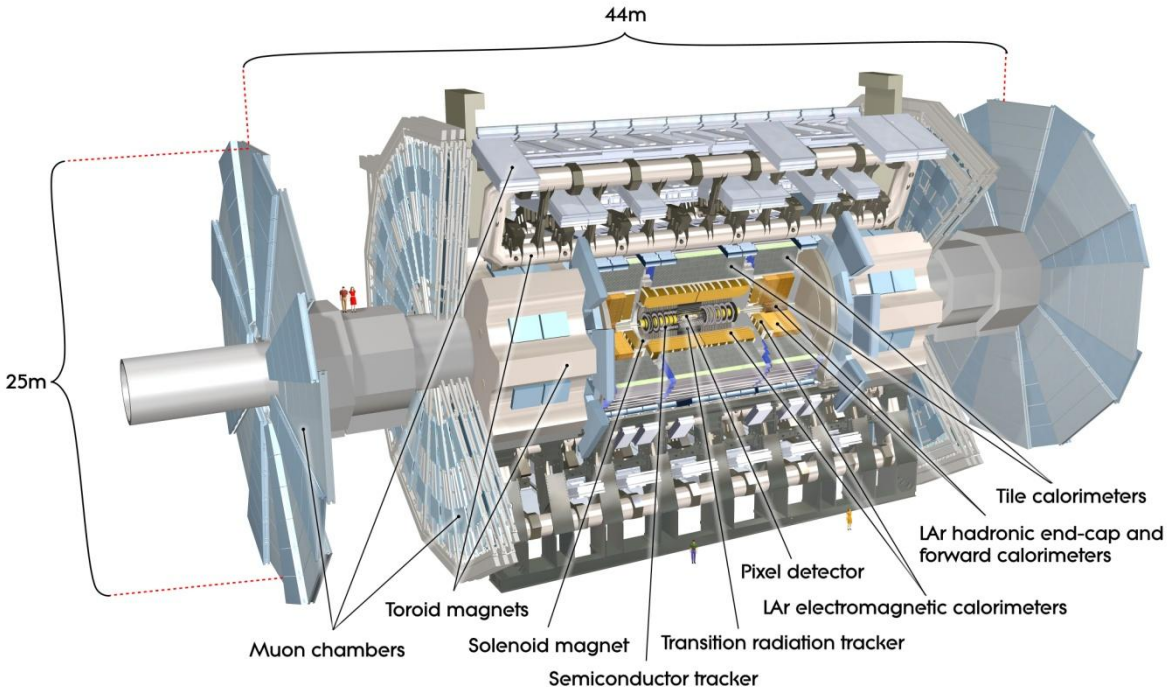

Fig. 2: The ATLAS detector and its description. (This figure is from[4])

1.4 Forward region ATLAS detector

Projects realized in the forward region of ATLAS are following: ALFA (Absolute Luminosity For ATLAS), LUCID (Luminosity measurement using a Cherenkov Integrating Detector), ZDC (A Zero Degree Calorimeter for ATLAS) and AFP (ATLAS Forward Protons) which is in phase of preparation.

The ALFA detector is designed to measure parameters of proton-proton scattering at small angles in the Coulomb-nuclear interference. The LUCID detector is designed to monitoring relative luminosity by using Cherenkov light. The ZDC detector is used for measurement of parameters of neutral particles at 0°(neutrons and photons in this case). The AFP detector is aimed to measure properties of new particles (Higgs boson, super symmetric particles). [6]

1.5 ALFA detector

ALFA detector is one of the ATLAS detectors in its forward region. It is represented by four stations with two Roman Pots per station. Each Roman Pot is occupied by tracking detector for measurement of proton trajectories close to the beam axis of LHC. Roman Pots with detectors approaches the beam axis in vertical coordinate up to 1.5 mm from the beam axis.

Two stations are placed on the A-side and two stations on the C-side of the ATLAS detector; see Fig 3, 237.408 m and 241.548 m away from ATLAS interaction point. Large distances and small divergence of the beam allows for detection of protons with very small momentum transfer. The naming convention of Roman Pots is shown at Fig. 3.

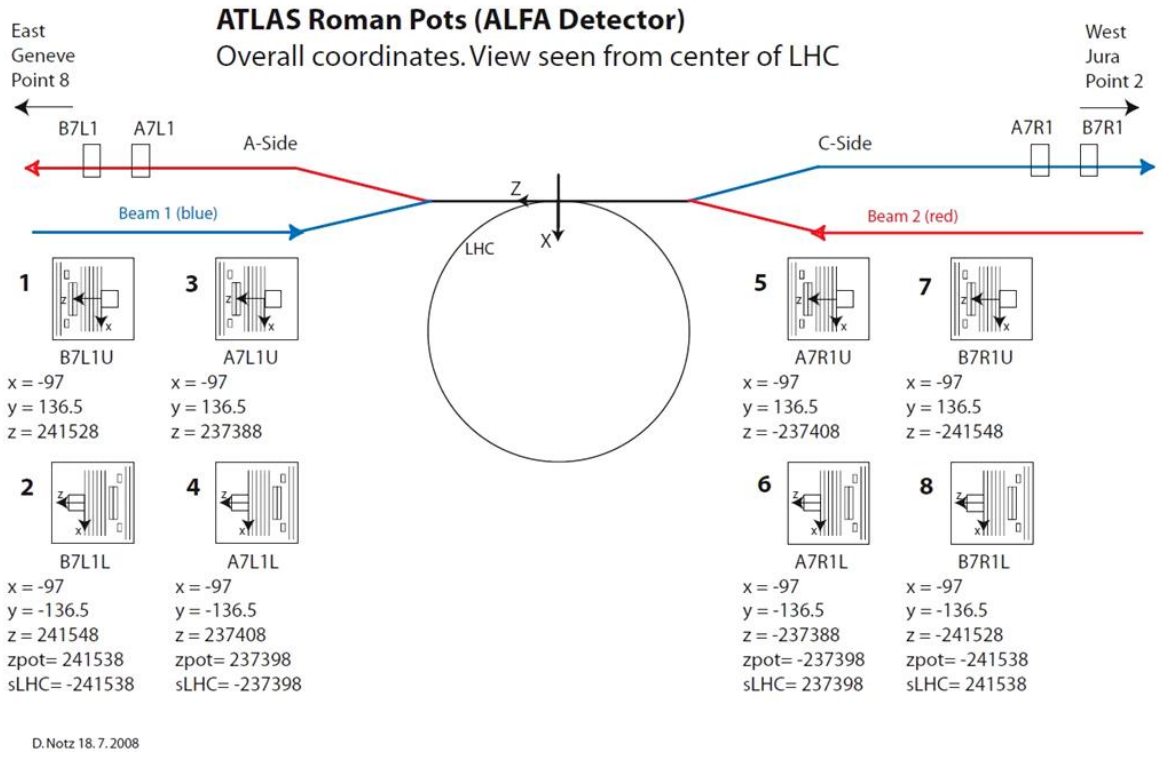

Fig. 3: The roman pots layout and naming convention [11].

The tracker detector of each Roman Pot contains three detection parts, Main Detector (MD) and two Overlap Detectors (OD, right and left). The Main detector detects both horizontal and vertical coordinates of passing proton. Overlap detectors are used to detect only vertical coordinate for alignment purposes.

The Main Detector consists of two sets of ten layers each made of 64 squared scintillation fibers. The layers are glued on titanium plates and fibers placed on the front sides are arranged under angle 90° with respect to those fibers placed on the back sides of the plate. Plates are staggered by 1/10 of the fiber size with respect to each other to increase resolution, see Fig. 4 details. [7]

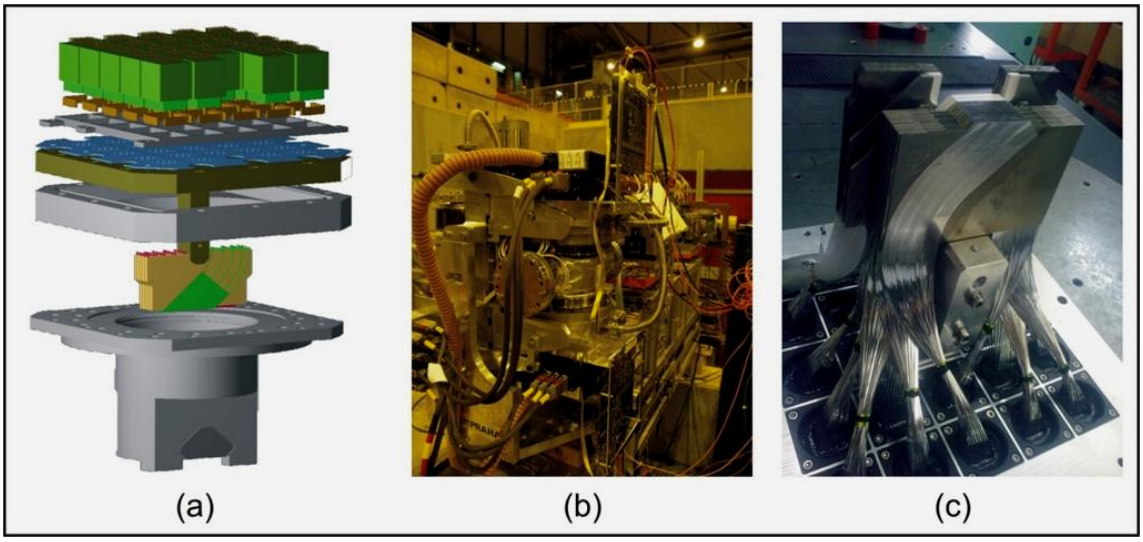

Fig. 4: (a) Software visualization of Roman pot (main detector is colored in green) (b) Picture of station containing two Roman Pots (c) Picture of fiber optics used in Roman Pot. [11]

1.6 Elastically scattered protons

Elastic scattering is the special case of proton-proton collisions. Elastic scattering is a process, where kinetic energy is conserved in central of mass system, but direction and propagation are modified by interaction with other particles, in our case protons, see Fig. 5.

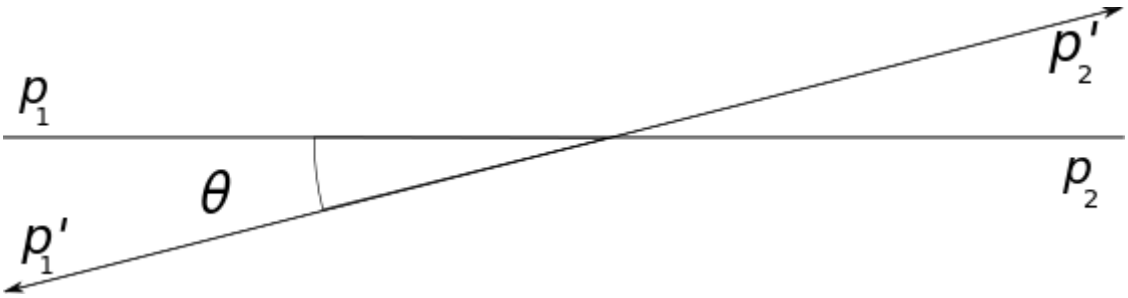

Fig. 5: Schema of elastic scattering and definition of scattering angle θ.

This definition put several constrains on detected protons. The main condition is that both protons have to survive interaction and both of the have to be detected simultaneously. Furthermore, the proton-proton scattering presumes that collision will be head-to-head in straight direction, which in turn implies the direction of outgoing protons is back-to-back and outgoing protons are moving along straight line but in opposite directions. We can consider an adept event on elastic scattering in case, when we have trigger signal in Roman Pots 1, 3, 6 and 8 or 2, 4, 5 and 7, see Fig 3. Those two series of detectors are called arms or elastic arms. This condition is not enough to recognize elastic scattering. We have to consider the angle which the particle came from. This can be done by comparing positions of detected proton from adjacent station. Specific methods are explained in the Chapter 3 [7, 8].

2. Mandelstam representation

2.1 Introduction

Dispersion relations for fixed momentum transfer for forward scattering can be easily presented in Mandelstam representation. It should be noted that we work with proton-proton scattering and those are scalar particles without isospin. We state $c = 1$ in whole text for easier calculating.

2.2 Kinematic features

The process containing two incoming and two outgoing scalar particles can be expressed by two scalar quantities, for example energy and scattering angle in central of mass system (CMS).

Consider the scattering of scalar particles and let the ingoing four-momenta be denoted as p_1 and p_2 and let the outgoing four-momenta be denoted as p_3 and p_4. The schema of scattering is shown in Fig. 6.

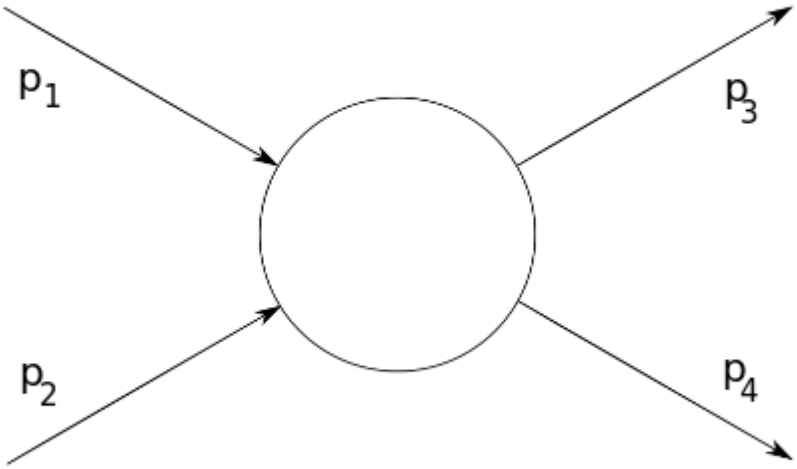

Fig.6: Schema of scattering interaction.

The conservation of energy and momentum can be written as

$$p_1 + p_2 = p_3 + p_4 \tag{1}$$

where

$$p_i^2 = -m_i^2 \quad (i = 1,2,3,4) \tag{2}$$

and m_i describes the mass of the particle. Products $p_i p_j$.form a set of six independent scalar variables. Four conditions are contained in Equation (1) which reduces the count of independent variables to two, as it was stated above. We can use energy and scattering angle in CMS system, but it can be easier to use energy and four-momentum transfer. Main advantage of use of energy and four momentum transfer is the invariance to the Lorentz transformation. Mandelstam variables are defined as three scalars defined as

$$s = -(p_1 + p_2)^2 = -(p_3 + p_4)^2, \tag{3}$$

$$t = -(p_1 - p_3)^2 = -(p_2 - p_4)^2, \tag{4}$$

$$u = -(p_1 - p_4)^2 = -(p_2 - p_4)^2. \tag{5}$$

These two sets of equations are the most frequently used in the literature. Following formula exists between three Mandelstam variables

$$s + t + u = m_1^2 + m_2^2 + m_3^2 + m_4^2 = \sum_i m_i^2. \tag{6}$$

This equation shows that only two of those parameters are independent. This formula can be proved as follows

$$\begin{aligned} s + t + u &= -(p_1 + p_2)^2 - (p_1 - p_3)^2 - (p_1 - p_4)^2 = \\ &= -3p_1^2 - p_2^2 - p_3^2 - p_4^2 - 2p_1(p_2 - p_3 - p_4) = \end{aligned} \tag{7}$$

$$= -p_1^2 - p_2^2 - p_3^2 - p_4^2 - 2p_1(p_1 + p_2 - p_3 - p_4) =$$

$$= -p_1^2 - p_2^2 - p_3^2 - p_4^2 = m_1^2 + m_2^2 + m_3^2 + m_4^2,$$

where the expression in brackets corresponds to Equation (1) and thus it has zero value. Applying Equation (2) we proved Equation (6). If we choose p_1 and p_2 as incoming particles, the representation in CMS system can be stated as

$$s = -(p_1 + p_2)^2 = (E_1 + E_2)^2 - (\boldsymbol{p_1} + \boldsymbol{p_2})^{\boldsymbol{2}} = E_c^2, \qquad (8)$$

$$t = -(p_1 - p_3)^2 = (E_1 - E_3)^2 - (\boldsymbol{p_1} - \boldsymbol{p_3})^{\boldsymbol{2}}. \qquad (9)$$

From these equations, it can be seen that *s* represents the square of the total energy in the CMS and *t* represents minus the square of four-momentum transfer, where p_1 and p_2 represents the incoming particles. The meaning of variables shifts among them if we change the incoming particles.

In the case of elastic scattering we consider two particles with masses $m_1 = m_3$ and $m_2 = m_4$. Elastic scattering is process where the kinetic energy is conserved but the direction can be changed by the interaction. Scattering angle is angle between incoming and outgoing direction of the particle (see Fig. 5). Let us consider again p_1 and p_2 as incoming particles. The scattering angle θ is defined as

$$p_{\boldsymbol{1}} \cdot p_{\boldsymbol{3}} = E_1 E_3 - |\boldsymbol{p_1}||\boldsymbol{p_3}| \cos\theta. \qquad (10)$$

Because we consider conservation of kinetic energy, we can state $E_1 = E_3$ and $E_1 = E_3$ as well as $|\boldsymbol{p_1}| = |\boldsymbol{p_3}|$ and $|\boldsymbol{p_2}| = |\boldsymbol{p_4}|$. This will help us to rewrite Equation (9) using Equation (10) into:

$$t = -(\boldsymbol{p_1} - \boldsymbol{p_3})^2 = -|\boldsymbol{p_1}|^2 - |\boldsymbol{p_3}|^2 + 2|\boldsymbol{p_1}||\boldsymbol{p_3}|$$

$$t = -2\boldsymbol{p}_c^2(1 - \cos\theta) \qquad (11)$$

where $\boldsymbol{p}_c$ is defined as $\boldsymbol{p}_c = |\boldsymbol{p}_1| = |\boldsymbol{p}_3|$ for one particle.

Angle θ is small enough for high (relativistic) energies and the Taylor expansion for the function cosine yields

$$t = -2p_c^2\left(1 - 1 + \frac{\theta^2}{2} - \frac{\theta^4}{24} + \frac{\theta^6}{720} - \cdots\right). \tag{12}$$

Because the value of θ is small, members with higher exponent than two can be neglected and the final expression for calculating the value of t can be written as follows

$$t = -p_c^2\theta^2. \tag{13}$$

This equation is used in every method described in next Chapter 3 [8].

2.3 Physical processes and Mandelstam variables

Considering interaction with antiparticles, we can imagine them as moving in time backwards. That makes the chose of ingoing and outgoing particles crucial for physical explanation. If we consider Fig. 6 again, it is not difficult to see that there are six processes, which can be grouped into three pairs, each pair corresponding to process and its reflected process.

If the spin and the isospin are not considered, then we can have analytic expression with any two Mandelstam variables which describes all six processes. Once again this is great advantage of the Mandelstam representation.

In the Mandelstam representation, it is customary to consider each process with its reversed process as a pair and refer to it as a single channel. If we denote the four-momenta of the particles once again as p_1, p_2, p_3 and p_4 and note the particles associated to them as 1, 2, 3 and 4 respectively, we can represent the interactions as follows:

Channel		Reaction	
u	I	$1+4 \rightarrow 2+3 \quad \text{and} \quad 2+3 \rightarrow 1+4$	(14)
t	II	$2+4 \rightarrow 1+3 \quad \text{and} \quad 1+3 \rightarrow 2+4$	(15)
s	III	$3+4 \rightarrow 1+2 \quad \text{and} \quad 1+2 \rightarrow 3+4$	(16)

These are two most popular notations used in literature to indicate the channels.

Mandelstam variable *t* can be used for calculating cross-section of collision interaction. The relation between variable *t* and total cross-section σ can be written as

$$\frac{d\sigma}{dt} = \frac{4\pi}{s}\frac{d\sigma}{d\Omega} \tag{17}$$

where Ω is the solid angle. This equation can be rewritten for particles as [8]

$$\frac{d\sigma}{dt} = \frac{4\pi}{s}\frac{1}{64\pi^2 s}|\mathcal{T}|^2 \tag{18}$$

where *t* and *s* are Mandelstam variables and $\mathcal{T}$ is the corresponding matrix element of Lorentz invariant reactance operator, which describes transition probability. This problematic is further explained in source [8].

3. Methods of calculation of Mandelstam variable *t* in forward regions of ATLAS detectors

3.1 Beam optics used in t-reconstruction

For reconstruction of variable *t*, we need to know how the trajectory of particle is described and transformed. Betatron-oscillation function β is the main variable which describes how the beam is divergent. It traditionally means a length where spot size is two times bigger than the one at the ATLAS Interaction Point. In frame on this thesis we focused on data $\beta^\star = 1$ km. Higher value of betatron-oscillation function imply closer distance of ALFA detectors to the beam which in turn could damage detectors.

The phase advance between the Interaction Point and the Roman Pots is important property of the optics. The arguments of transport matrix can be simplified if the phase advance in the vertical plane is 90°. Furthermore, if we manage to have the phase advance in the horizontal plane 180°, our calculations will simplify significantly.

Transport matrix is a tool for describing trajectory of charged particle within the Large Hadron Collider through the magnetic lattice. The transport matrix transforms coordinates $u^\star$ and momenta $p^\star$ in the Interaction Point to coordinates u at any position in plane transversal to the nominal orbit *s* along the ring at any position. This dependence can be written as:

$$\begin{pmatrix} u(s) \\ u'(s) \\ \dfrac{\Delta p(s)}{p} \end{pmatrix} = M \begin{pmatrix} u^\star \\ u^{\star\prime} \\ \dfrac{\Delta p^\star}{p} \end{pmatrix} \tag{19}$$

where

$$M = \begin{pmatrix} \sqrt{\frac{\beta}{\beta^\star}}(\cos\Psi + \alpha^\star \sin\Psi) & \sqrt{\beta\beta^\star}\sin\Psi & D \\ \frac{(\alpha^\star - \alpha)\cos\Psi - (1+\alpha\alpha^\star)\sin\Psi}{\sqrt{\beta\beta^\star}} & \sqrt{\frac{\beta}{\beta^\star}}(\cos\Psi + \alpha\sin\Psi) & D' \\ 0 & 0 & 1 \end{pmatrix}, \quad (20)$$

and D represents dispersion of the beam, D' is derivative of dispersion, α is derivative of betatron-oscillation function and Ψ is phase advance of the betatron-oscillation function. For elastic scattering the value of dispersion is small enough to be neglected. If this neglecting is considered, transport matrix can be written in form

$$\mathbf{M} = \begin{pmatrix} M_{11} & M_{12} \\ M_{21} & M_{22} \end{pmatrix}. \quad (21)$$

Coordinates of the particle can be calculated as follows:

$$u = M_{11}u^\star + M_{12}u^{\star\prime} = \\ = \sqrt{\frac{\beta}{\beta^\star}}(\cos\Psi + \alpha^\star \sin\Psi)u^\star + \sqrt{\beta\beta^\star}\sin\Psi\, u^{\star\prime} \quad (22)$$

Because the beams 1 and 2 vary slightly, coordinates *x* and *y* are independent and fluctuate, the transport matrix is dependent on position *s* and 32 different matrix elements are needed to describe whole ALFA set-up.

In Equation (22), it can be seen that position in Roman Pot is given by vertex position $u^\star$ and scattering angle $\theta_u^\star = u^{\star\prime}$. For easier calculations of scattering angle the parallel-to-point focusing is used, which sets the phase advance Ψ in vertical plane close to 90° and for the high values of $\beta^\star$ optics is α small enough to be neglected. Scattering angle is given in vertical plane as:

$$\theta_{\mathrm{y}}^{\star} = \frac{y}{M_{12}^{y}}, \tag{23}$$

where

$$M_{12}^{\mathrm{y}} = L_{\mathrm{eff,y}} = \sqrt{\beta_{\mathrm{y}}\beta_{y}^{\star}}\sin\Psi_{\mathrm{y}}, \tag{24}$$

and $\boldsymbol{L_{\mathrm{eff,y}}}$ is length of lever arm which varies for each Roman Pot. For horizontal plane the lever arm is defined in similar way but the phase advance of the betatron-oscillation function $\boldsymbol{\Psi}$ is close to the 180° [7,9].

3.2 Subtraction

Subtraction is main method used on ALFA detector and is based on fact that elastic scattered particles are outgoing in opposite directions (back-to-back particles). Scattering angle detected by one side of arm (for example arm with stations 1 and 3) has to be same in absolute value and opposite in sign to the angle detected in the opposite side of arm (in our example stations 6 and 8). To maximize the lever arm M_{12} in the vertical plane we have to optimize optics to obtain the smallest possible scattering angles. Because of those conditions, we can write values of angle and coordinates as follows (indexes describe example):

$$\begin{aligned} \theta_1^{\star} = -\theta_8^{\star} = \theta^{\star}, \qquad u_1^{\star} = -u_8^{\star} = u^{\star}, \\ \theta_3^{\star} = -\theta_6^{\star} = \theta^{\star}, \qquad u_3^{\star} = -u_6^{\star} = u^{\star}. \end{aligned} \tag{25}$$

We can write following formula using Equation (22) and stating difference between coordinates observed in one side of arm and other side of:

$$\begin{aligned} u_1 - u_8 = M_{11;1}u^{\star} + M_{12;1}\theta_{\mathrm{u}}^{\star} - M_{11;8}u^{\star} + M_{12;8}\theta_{\mathrm{u}}^{\star} \\ u_3 - u_6 = M_{11;3}u^{\star} + M_{12;3}\theta_{\mathrm{u}}^{\star} - M_{11;6}u^{\star} + M_{12;6}\theta_{\mathrm{u}}^{\star}. \end{aligned} \tag{26}$$

In this equation, we used simplification that divergence can be neglected but its influence can be seen in the difference between scattering angles observed in one side and opposite side of arm, which worsens the resolution of the reconstructed angle slightly. The matrix element M_{11} is approximately same for both beams, which helps us to simplify Equation (26) to:

$$\begin{aligned} u_1 - u_8 &\approx 2M_{12}\theta_{\mathrm{u}}^{\star}, \\ u_3 - u_6 &\approx 2M_{12}\theta_{\mathrm{u}}^{\star}. \end{aligned} \tag{27}$$

This modification eliminates the dependence on unknown vertex position.

At this point method yields excellent reconstruction of the vertical scattering angle component, but for horizontal component we have larger asymmetry between beams. This is integrated through next modification:

$$\begin{aligned} \theta_{\mathrm{u}}^{\star} &= \frac{u_1 - u_8}{M_{12;1} + M_{12;8}} \\ \theta_{\mathrm{u}}^{\star} &= \frac{u_3 - u_6}{M_{12;3} + M_{12;6}}. \end{aligned} \tag{28}$$

This formula is calculated for *x* and *y* separately and for inner and outer stations thus we have two values of *t* given per event. When we combine equations (28) and (13) the formulas yields:

$$\begin{aligned} -t_{\mathrm{inn}} &= \left[\left(\theta_{\mathrm{x,inn}}^{\star}\right)^2 + \left(\theta_{\mathrm{y,inn}}^{\star}\right)^2\right] p^2, \\ -t_{\mathrm{out}} &= \left[\left(\theta_{\mathrm{x,out}}^{\star}\right)^2 + \left(\theta_{\mathrm{y,out}}^{\star}\right)^2\right] p^2. \end{aligned} \tag{29}$$

The value of the variable *t* is calculated as arithmetical average from those two values [7]

$$t = \frac{t_{\mathrm{inn}} + t_{\mathrm{out}}}{2}. \tag{30}$$

3.3 Local angle

For calculation of the variable *t*, the angle of the trajectory measured between inner and outer station can be used. This method has advantage in lesser sensitivity to uncertainties in Ψ. On the other hand, the resolution is not as good as in the subtraction method due to the short distance between stations. The basic formula is usually stated as (in this equation we use same indexes to resolve sides of the arm):

$$\theta_{\mathrm{u}}^{\star} = \frac{\theta_{\mathrm{u};1,3} - \theta_{\mathrm{u};6,8}}{M_{22;1,3} + M_{22;6,8}}. \tag{31}$$

In this equation, we again use same procedure to avoid the dependence on vertex position like in previous subtraction method. This method comes with only one reconstructed value of *t* per event due only one local angle between stations, and the transport matrix element M_{22} is same for inner and outer stations.

The reconstructed value of *t* is gained by following statement

$$-t = \left[(\theta_{\mathrm{x}}^{\star})^2 + \left(\theta_{\mathrm{y}}^{\star}\right)^2\right] p^2. \tag{32}$$

3.4 Local subtraction

The local subtraction method is similar to the subtraction method, but calculates value of *t* in each side separately. The scattering angle in one side is calculated by formula:

$$\theta_{\mathrm{u}}^{\star} = \frac{M_{11;1}u_3 - M_{11;3}u_1}{M_{11;1}M_{12;3} + M_{11;3}M_{12;1}}. \tag{33}$$

The value of *t* is calculated in same way as in the local angle method by using Equation (30) and it is combined afterwards. Method is not dependent on vertex position in exchange for the worsen resolution in the vertical plane.

3.5 Lattice method

Last method mentioned in this work uses inverted transport matrix for calculating scattering angle from reconstructed positions and local angle. Scattering angle is calculated from following statement:

$$\begin{pmatrix} u^{\star} \\ \theta_u^{\star} \end{pmatrix} = \mathbf{M}^{-1} \begin{pmatrix} u \\ \theta_u \end{pmatrix} \tag{34}$$

as

$$\theta_u^{\star} = M_{12}^{-1} u + M_{22}^{-1} \theta_u \, . \tag{35}$$

The transport matrix inversion can be applied on every Roman Pot in arm, thus this method can give up to four values of variable *t* per event. Once again the value of variable *t* is given as an arithmetical average.

4. Reconstruction efficiency

4.1 Introduction

The reconstruction efficiency describes how good our algorithm is for the reconstruction of the *x* and *y* positions of the particle in ALFA detectors. Reconstruction algorithm is primarily used for the calculation of the position of protons for the elastic events. Those events are characteristic by back-to-back topology as it was mentioned in Chapter 1.6. Expected cases describing elastic scattering are those, where there are reconstructed positions in all four detectors corresponding to the elastic arm. But in many cases the reconstruction algorithm is not able to calculate the right positions due to showers, pile-up and background events. In those cases there can be more than one track in the detector and the reconstruction algorithm may fail the reconstruction. In this chapter we describe the calculation of the reconstruction efficiency from gathered data [7].

4.2 Definition of the reconstruction efficiency

As it was mentioned above, the reconstruction efficiency is described by elastic events with successful reconstruction of position and events where the reconstruction algorithm fails. This can be written as:

$$\varepsilon_{\mathrm{rec}}(t) = \frac{N_{\mathrm{rec}}(t)}{N_{\mathrm{rec}}(t) + N_{\mathrm{fail}}(t)} \tag{36}$$

where $\varepsilon_{\mathrm{rec}}$ is reconstruction efficiency, N_{rec} is number of events where the reconstruction algorithm was successful (there is at least one reconstructed track in every pot in elastic arm) and N_{fail} is number of events where reconstruction algorithm failed. In general all those parameters depend on Mandelstam parameter *t*. The elastic events are independent on arm, thus the reconstruction efficiency is calculated for each arm separately.

The possible reconstruction cases are related to triggers. The ALFA triggers for each Roman Pot have efficiency around 99.9%, thus we can consider them as a reference for reconstruction. The fully reconstructed elastic event can be written as X/X, where the first digit corresponds to the number of reconstructed tracks in corresponding pots in arm and the second digit corresponds to the number of trigger signals from each pot. Case 4/4

is the most important, because describes fully reconstructed elastic event (four pots with reconstructed tracks, four pots with trigger signal). The other combinations are 3/4 (three pots with reconstructed track, four pots with trigger signal), 2/4 (two pots on one side with reconstructed track, four pots with trigger signal), 1+1/4 (two pots each on one side with reconstructed track, four pots with trigger signal), 1/4 (one pot with reconstructed track, four pots with trigger signal) and 0/4(no pot with reconstructed track, four pots with trigger signal). The case 4/4 is event where our reconstruction algorithm was successful. Reconstruction algorithm fails for all other combinations. We can rewrite Equation (36) with these assumptions into the next statement

$$\varepsilon_{\mathrm{rec}}(t) = \\ = \frac{N_{4/4}(t)}{N_{4/4}(t) + N_{3/4}(t) + N_{2/4}(t) + N_{1+1/4}(t) + N_{1/4}(t) + N_{0/4}(t)} \tag{37}$$

where the ratio $\mathrm{k}/4$ describes cases mentioned above.

The dependence on parameter *t* can be eliminated by using following formula

$$N_{\mathrm{k}/4} = \int_{-\infty}^{0} N_{\mathrm{k}/4}(t)\mathrm{d}t \tag{38}$$

where the number k describes the number of pots with reconstructed tracks, which corresponds to the cases mentioned above. The formula (37) can be rewritten into the next statement, where the elimination of the dependence on the Mandelstam parameter *t* is accomplished:

$$\varepsilon_{\mathrm{rec}} = \frac{N_{4/4}}{N_{4/4} + N_{3/4} + N_{2/4} + N_{1+1/4} + N_{1/4} + N_{0/4}} \tag{39}$$

Reconstruction efficiency of ALFA detectors was measured to be close to 100% in test beams for minimum ionizing particles. The reason of the reconstruction inefficiency has two main sources; first there were too many tracks from showers, beam halo etc., second the trajectory of the particle was too close to the edge and there were not enough of fibers hit in the detector. The first source of inefficiency (too many tracks) has to be

included in calculations. On the other hand, the second source (position of the particle) should be excluded because it is the acceptance effect [7] (more information about the acceptance can be found in [7]).

5. Experimental setup

5.1 Data collection

Protons used for collisions are grouped in bunches and they move along the LHC ring together. This conformation is used for improving the probability of collision. Particles measured in the ATLAS detector collide in the ATLAS Interaction Point. The frequency of collision is 40 MHz and the measured data for each bunch are 1-1.5 MB large [2]. It is impossible to store all gathered data with present technologies and that is why a trigger system is used. The aim of the trigger system is to filter and store events of interest for physics.

Data collection is done on stable beams which they have parameters stable in time and precisely stated. A run is a process of collection within a long time period. The run is divided into lumiblocks, short time period slices (around one minute), where a change of run parameters in time is negligible [7, 9].

Here we deal with run no. 213268 started 24th October 2012 at 19:28, with the end 25th October 2012 at 8:34.

5.2 Data storage and processing

Raw data gathered in the one-kilometer run 213268 are digitalized and saved electronically. Then data are rewritten to a special format for further processing in files called Ntuples (ROOT format). Ntuples are structured into several trees (main files). In those trees are separated into groups based on their physics meaning and DAQ pertinence. For example, data used for processing position of proton are stored in tracking data tree. Every tree consists of branches (subfiles) and leaves which describe one particular parameter. For example, there is a branch called x_Det, in the tracking data tree for ALFA output, which describes horizontal position in corresponding ALFA detector.

Ntuples are processed by specialized program called ROOT, which is primarily designed to analyze event based data. The ROOT is a multiplatform freeware utility. All figures in Chapter 6 and 7 are made in this program. More information about ROOT can be found in source [10].

5.3 Reconstruction efficiency analysis

Information from tracking data and event header tree is needed to calculate reconstruction efficiency. Raw data have to be filtered on elastic events before main reconstruction efficiency is calculated. Filtration of events is processed in several steps. Event selection steps are:

- Selection on good lumiblocks.

  Selected lumiblocks have to accomplish several conditions. First, they have to be flagged as physics ready lumiblocks. Second, the lumiblock length has to be at least 60 seconds and last, the energy of the lumiblock is over 3.9 TeV.

- Filtering inelastic events.

  The ATLAS detector has few more forward region components, each for detection of different situations. Inelastic event can be recognized from trigger signal from LUCID or MBTS.

- BCId filtering.

  Colliding bunches are described by BCId (Bunch Crossing Identifier). Reconstruction efficiency is calculated from nominal bunches, which are recognized by the right BCId. Furthermore, there is placed condition on pairing. Unpaired bunches cannot collide and should be excluded as well.

- Trigger signal filter.

  The trigger signals are considered as reference, as it was mentioned before. Only those events with four trigger signal corresponding to considered arm may pass this filter.

- Case recognition of reconstruction.

  This step sorts events by their reconstruction case; the knowledge of all case counts is needed for calculating reconstruction efficiency later.

- Multiplicity filter.

  In the case, that there is at least one not reconstructed track, a condition is placed on Roman Pot without reconstruction. Total multiplicity (multiplicity of fibers hits summed over all layers in the Roman Pot) has to be over five to pass this filter step. This excludes events, where there is too few information for successful reconstruction.

- Edge cut filter.

  This filter places condition on vertical coordinate. Events with vertical coordinate lesser than the vertical position of edge of detector have to be excluded. This filtering step contains safety cut away from the edge. This filter removes the acceptance effect.

Survived events are counted and summarized for each case and final reconstruction efficiency is calculated from those values.

5.4 Data used for analysis of Mandelstam variable *t*

Analysis of Mandelstam variable *t* can't be made on raw data without alignment. The alignment on the run 213268 is not well understood yet and the analysis cannot be made. This problem was solved by using simulation data where all events are elastic. These data are simulated by Monte Carlo simulation algorithm only for purposes of this work. Simulated data have same optics calibration like run 213268 and the expectations should correspond to measured data.

Simulated data are stored again in Ntuple format file and processed by ROOT software.

6. Reconstruction efficiency analysis

6.1 Introduction

Reconstruction efficiency has been stated for one-kilometer optics run 213268 for nominal bunches. There were two nominal bunches types in this run recognized by BCId. BCId is Bunch Crossing Identifier, which helps us to distinguish between nominal and other bunches. Nominal bunches are required to study physics on collider. Nominal bunch have to fulfill several parameters like intensity (population of protons in bunch), luminosity (number of particles per cm squared per second) and crossing betatron oscillation function value. In the run 213268 there are three nominal bunches with BCId 1, 101 and 1886. Bunches with BCId 1 have too low intensity, which leads to unacceptable signal to noise ratio for analysis. Whole analysis is made for each nominal bunch separately and then both together. Analysis has been made by script RecoEff.C. This script can be found on attached CD which is part of this work.

6.2 Lumiblock statistics for run 213268

Chapter 5 descries method of events selection. Lumiblock event filtering is one of its first steps. This run is designed for particles colliding with energy 4 TeV, but not all lumiblocks fulfill this condition. Distribution of lumiblock energy is presented on Fig.7.

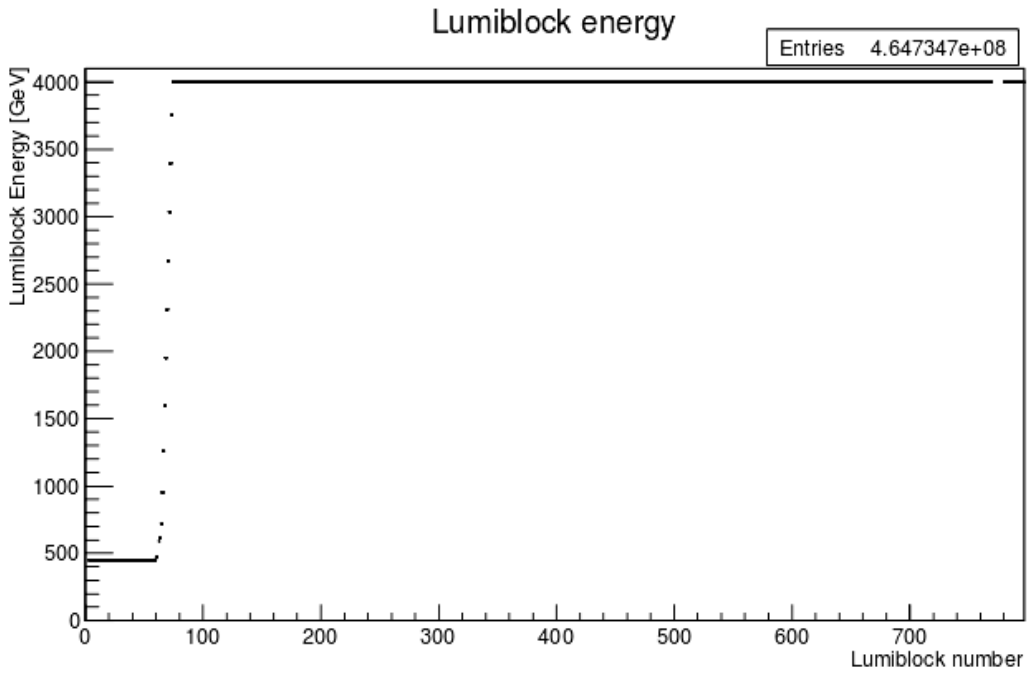

Fig.7: Histogram of energy of lumiblocks.

From Fig.7 it can be seen that lumiblocks at the beginning of run have very low energy of protons and have to be excluded from analysis.

There is one more condition placed on lumiblocks. Lumiblock length have to be over 60 seconds. Distribution of lumiblock length is shown on Fig.8.

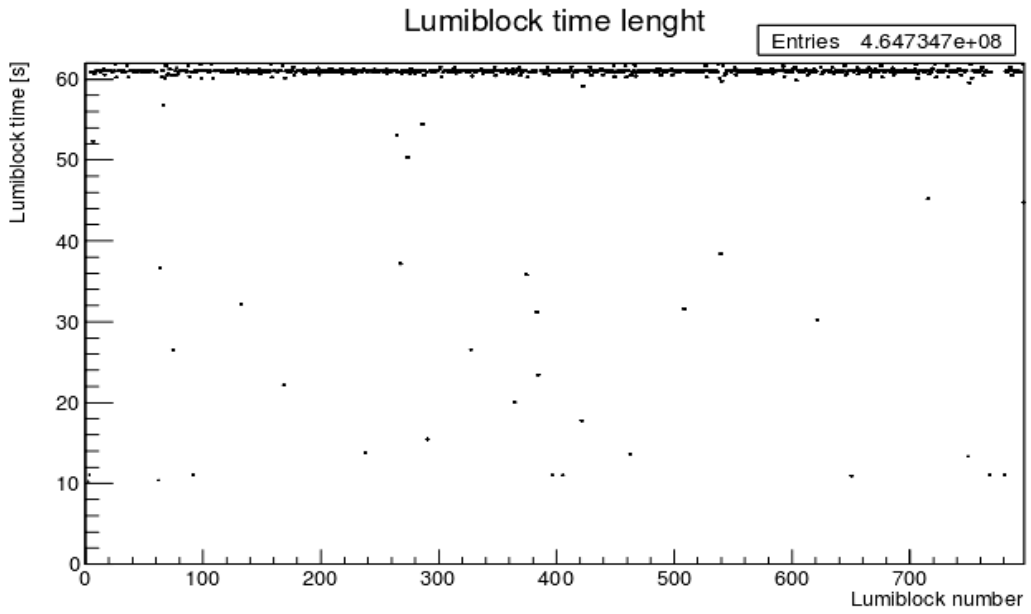

Fig.8: Histogram of time length of lumiblocks.

We can see that not all lumiblocks have time length over 60 seconds. All lumiblocks which do not meet the minimum duration requirements are dumped.

6.3 Reconstruction efficiency analysis for nominal bunch with BCId 101

Reconstruction efficiency has been calculated as it was described in Chapter 4. Raw data had to be filtered first. Selection of good events proceeds as it was mentioned in Chapter 5. Each step of filtering is described in Tab.1.

Tab.1: ***Event counts in selection steps for BCId 101***

Number of imputed events	464734704
Number of events after BCId selection	122305200
Number of events after lumiblock selection	90436916
Number of events after non-elastic filter	49417605
Number of events after ALFA trigger selection	4258279
Number of events after multiplicity and edge cut selection	1790287

Events which have passed the selection are sorted in corresponding reconstruction case (combination), see Chapter 4 for more information. Combinations are presented in Tab.2 for each arm and case separately.

Tab.2: ***Event counts of reconstruction cases for BCId 101***

Case	Arm	Number of Roman pot without reconstructed track	Number of events
4/4	1368	-	123312
4/4	2457	-	192044
3/4	1368	1	20317
3/4	1368	3	7771
3/4	1368	6	13401
3/4	1368	8	36762
3/4	2457	2	47738
3/4	2457	4	10995
3/4	2457	5	13202
3/4	2457	7	48814
2/4	1368	6, 8	123273
2/4	1368	1, 3	47157
2/4	2457	5, 7	165943
2/4	2457	2, 4	100133
1+1/4	1368	3, 6	3945
1+1/4	1368	3, 8	9971
1+1/4	1368	1, 6	6524
1+1/4	1368	1, 8	17997
1+1/4	2457	4, 5	1551
1+1/4	2457	4, 7	5371
1+1/4	2457	2, 5	5474
1+1/4	2457	2, 7	22976
1/4	1368	3, 6, 8	39641
1/4	1368	1, 6, 8	70084
1/4	1368	1, 3, 8	59861
1/4	1368	1, 3, 8	22243
1/4	2457	4, 5, 7	21631
1/4	2457	2, 5, 7	83859
1/4	2457	2, 4, 7	51430
1/4	2457	2, 4, 5	13326
0/4	1368	1, 3, 6, 8	219794
0/4	2457	2, 4, 5, 7	18374

All cases presented above are summarized and reconstruction efficiency is calculated for each arm separately and for both together. Results are shown in Tab.3.

Tab.3: ***Reconstruction efficiency for BCId 101***

Reconstruction efficiency	18%
Reconstruction efficiency in arm 1368	15.%
Reconstruction efficiency in arm 2457	20%

The summary statistics for particular cases is presented in Tab.4.

Tab.4: ***Reconstruction cases for BCId 101***

Case	Number of events	Percentage count
4/4	315356	18%
3/4	199000	11.%
2/4	436506	24.%
1+1/4	73809	4.%
1/4	362075	20%
0/4	403541	23%

6.4 Reconstruction efficiency analysis for nominal bunch with BCId 1886

Reconstruction efficiency for nominal bunches with BCId 1886 is done in same way as for nominal bunches with BCId 101. In Tab.5 is described event selection process.

Tab.5: ***Event counts in selection steps for BCId 1886***

Number of imputed events	464734704
Number of events after BCId selection	116534334
Number of events after lumiblock selection	85487951
Number of events after non-elastic filter	45530819
Number of events after ALFA trigger selection	3483999
Number of events after multiplicity and edge cut selection	1544560

Events which have passed the selection are sorted in corresponding reconstruction case as it was described in Chapter 4. Number of events for every case is presented in Tab.6.

Tab.6: ***Event counts of reconstruction cases for BCId 1886***

Case	Arm	Number of Roman pot without reconstructed track	Number of events
4/4	1368	-	106285
4/4	2457	-	161730
3/4	1368	1	16089
3/4	1368	3	6146
3/4	1368	6	10620
3/4	1368	8	27873
3/4	2457	2	38389
3/4	2457	4	8918
3/4	2457	5	10142
3/4	2457	7	35463
2/4	1368	6, 8	104459
2/4	1368	1, 3	36449
2/4	2457	5, 7	143523
2/4	2457	2, 4	80583

1+1/4	1368	3, 6	3069
1+1/4	1368	3, 8	6775
1+1/4	1368	1, 6	4764
1+1/4	1368	1, 8	11875
1+1/4	2457	4, 5	1182
1+1/4	2457	4, 7	3579
1+1/4	2457	2, 5	4076
1+1/4	2457	2, 7	13696
1/4	1368	3, 6, 8	34772
1/4	1368	1, 6, 8	69789
1/4	1368	1, 3, 8	39802
1/4	1368	1, 3, 8	16819
1/4	2457	4, 5, 7	19163
1/4	2457	2, 5, 7	90874
1/4	2457	2, 4, 7	31485
1/4	2457	2, 4, 5	9869
0/4	1368	1, 3, 6, 8	209573
0/4	2457	2, 4, 5, 7	186728

The summary for reconstruction efficiency for BCId 1886 is shown in Tab.7 for each arm and combined.

Tab.7: ***Reconstruction efficiency for BCId 1886***

Reconstruction efficiency	17.%
Reconstruction efficiency in arm 1368	15.%
Reconstruction efficiency in arm 2457	19.%

The summary statistics for particular cases are presented in Tab.8.

Tab.8: ***Reconstruction cases for BCId 1886***

Case	Number of events	Percentage count
4/4	268015	17%
3/4	153640	10%
2/4	365014	24%
1+1/4	49016	3%
1/4	312573	20%
0/4	396302	26%

6.5 Reconstruction efficiency analysis for both nominal bunches

In this chapter, results are presented for nominal bunches with BCId 101 and 1886 processed together. Event selection for both bunches are shown in Tab.9.

Tab.9: ***Event counts in selection steps for BCId 101 and 1886 together***

Number of imputed events	464734704
Number of events after BCId selection	238839534

Number of events after lumiblock selection	175924867
Number of events after non-elastic filter	94948424
Number of events after ALFA trigger selection	7742278
Number of events after multiplicity and edge cut selection	3334847

Events which have passed the selection are again sorted in corresponding reconstruction case as it was described in Chapter 4. Event counts all combination are presented in Tab.10.

Tab.10: ***Event counts of reconstruction cases for BCId 101 and 1886 together***

Case	Arm	Number of Roman pot without reconstructed track	Number of events
4/4	1368	-	229597
4/4	2457	-	353774
3/4	1368	1	36406
3/4	1368	3	13197
3/4	1368	6	24021
3/4	1368	8	64635
3/4	2457	2	86127
3/4	2457	4	19913
3/4	2457	5	23344
3/4	2457	7	84277
2/4	1368	6, 8	227732
2/4	1368	1, 3	83606
2/4	2457	5, 7	309466
2/4	2457	2, 4	180716
1+1/4	1368	3, 6	7014
1+1/4	1368	3, 8	16746
1+1/4	1368	1, 6	11288
1+1/4	1368	1, 8	29872
1+1/4	2457	4, 5	2733
1+1/4	2457	4, 7	8950
1+1/4	2457	2, 5	9550
1+1/4	2457	2, 7	36672
1/4	1368	3, 6, 8	74413
1/4	1368	1, 6, 8	139873
1/4	1368	1, 3, 8	99663
1/4	1368	1, 3, 8	39062
1/4	2457	4, 5, 7	40794
1/4	2457	2, 5, 7	174733
1/4	2457	2, 4, 7	82915
1/4	2457	2, 4, 5	23195
0/4	1368	1, 3, 6, 8	429368
0/4	2457	2, 4, 5, 7	370475

The summary for reconstruction efficiency for BCId 101 and1886 is shown in Tab.11 for each arm and combined.

Tab.11: ***Reconstruction efficiency for BCId 101 and 1886***

Total reconstruction efficiency	17%
Total reconstruction efficiency in arm 1368	15%
Total reconstruction efficiency in arm 2457	20%

The summary statistics for particular cases are presented in Tab.12.

Tab.12: ***Reconstruction cases for BCId101 and 1886***

Case	Number of events	Percentage count
4/4	268015	17%
3/4	153640	11%
2/4	365014	24%
1+1/4	49016	4%
1/4	312573	20%
0/4	396302	24%

Total reconstruction efficiency expectations were around 70 - 80%. My results are worse around 15 - 20%. This difference between expectation and result leaded to confrontation with results from run 191373 (run with 90 m optics). In this run, reconstruction efficiency was calculated and well understood. Script was modified for run 191373 for validation. Results are shown in Tab.13. together with results given by a existing CERN script (taken from [7]).

Tab.13: ***Comparison of total reconstruction efficiency for run 191373***

	Reconstruction efficiency
Result from my script for arm 1368	88%
Result from my script for arm 2457	87%
Result from CERN script for arm 1368	90%
Result from CERN script for arm 2457	88%

It is clear from the Tab.13. that my script results correspond to existing CERN script results. The difference between results is caused by better understanding of run 191373, especially understanding of alignment. Results from my script can be considered good for first analysis on raw data.

6.5 Multiplicity investigation

6.5.1 Total multiplicity investigation

Showers are the main sources of reconstruction inefficiency as it was mentioned in Chapter 4. Amount of showers in run 213268 is expected to be higher in comparison with run 191373 due to higher energy of colliding proton bunches. Total multiplicity is used to investigate showers activity. Total multiplicity is defined as the number of elements with signal per Roman Pot. Roman Pot has ten titanium plates with 64 fibers glued on each side of plate as it was mentioned before (see Chapter 1.5). The maximal value of total multiplicity is 1280, which means every element in Roman Pot have signalized a hit. Single particle generate up to 20 hits per Roman Pot, one hit per layer.

The reconstruction algorithm fails in cases, where there are too many hits. It helps us to understand what happened in Roman Pots without reconstructed track in cases where reconstruction algorithm fails. It is obvious that reconstruction algorithm have to fail if the products of shower hit high value of elements in the Roman Pot. Distribution of total multiplicity in Roman Pots without reconstruction for whole run is presented on Fig.9.

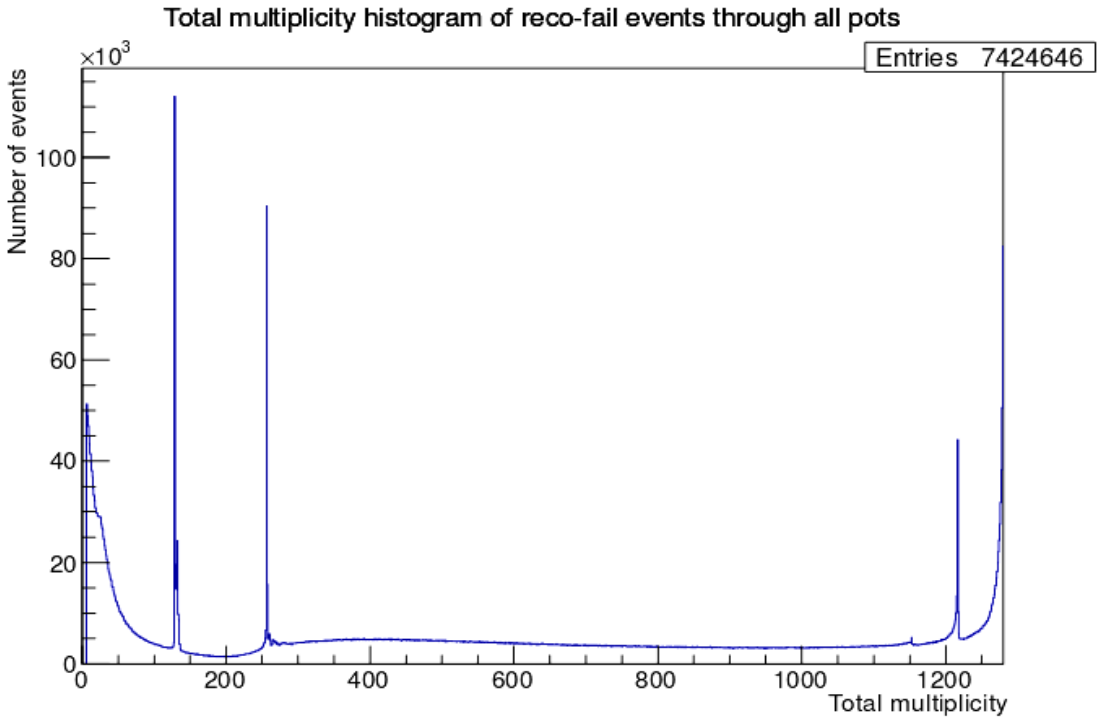

Fig.9: Total multiplicity histogram for all events with at least one Roman Pot fails the reconstruction process.

Total multiplicity in particular Roman Pots for events without reconstructed track is shown on the Fig.10 for both nominal bunches for A side.

6.5.2 Total multiplicity investigation for particular Roman Pots

Distributions of total multiplicity in particular Roman Pots are shown in Fig. 10 (side A) and Fig. 11 (side C) for events without reconstructed track for both nominal bunches.

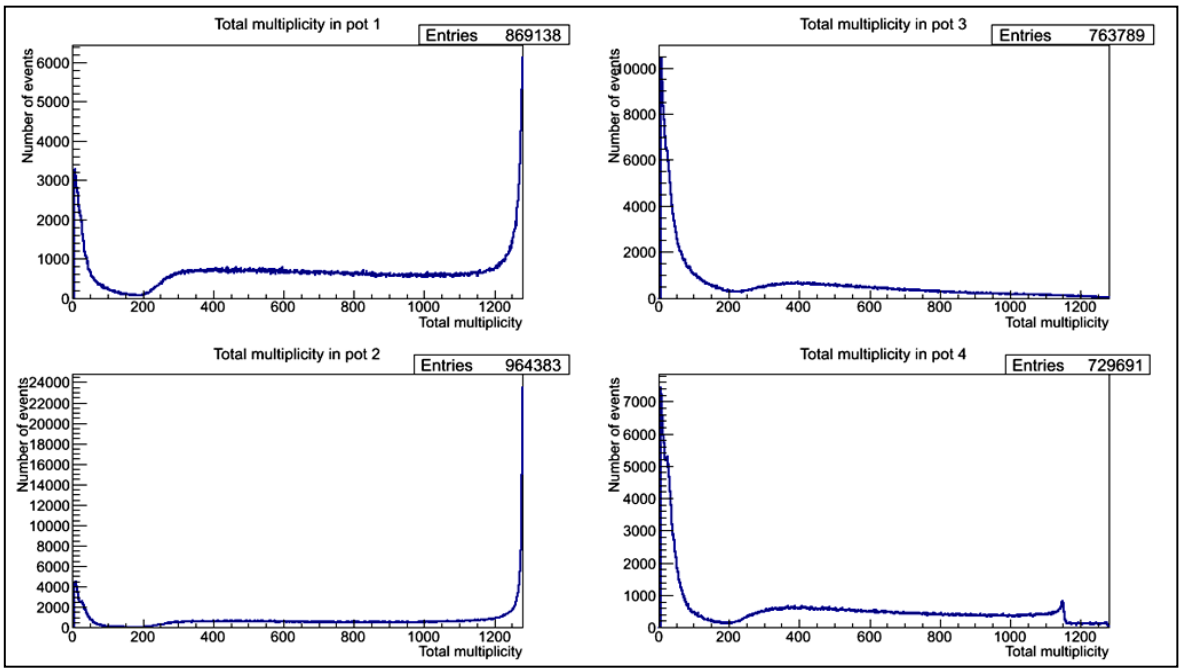

Fig.10: Total multiplicity for particular Roman Pots on A side for events without reconstructed track for both nominal bunches.

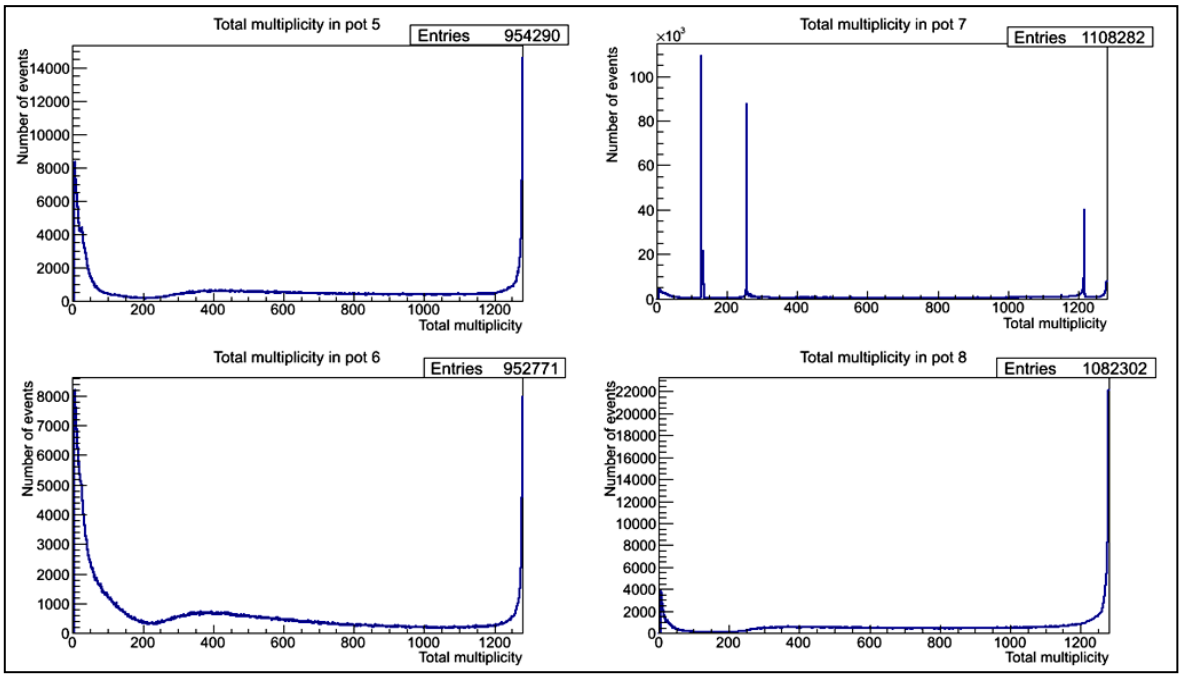

Fig.11: Total multiplicity for particular Roman Pots on C side for events without reconstructed track for both nominal bunches.

Distributions of multiplicity in particular Roman Pots for BCId 101 are presented in Fig. 12 (side A) and Fig. 13 (side C) for events without reconstruction.

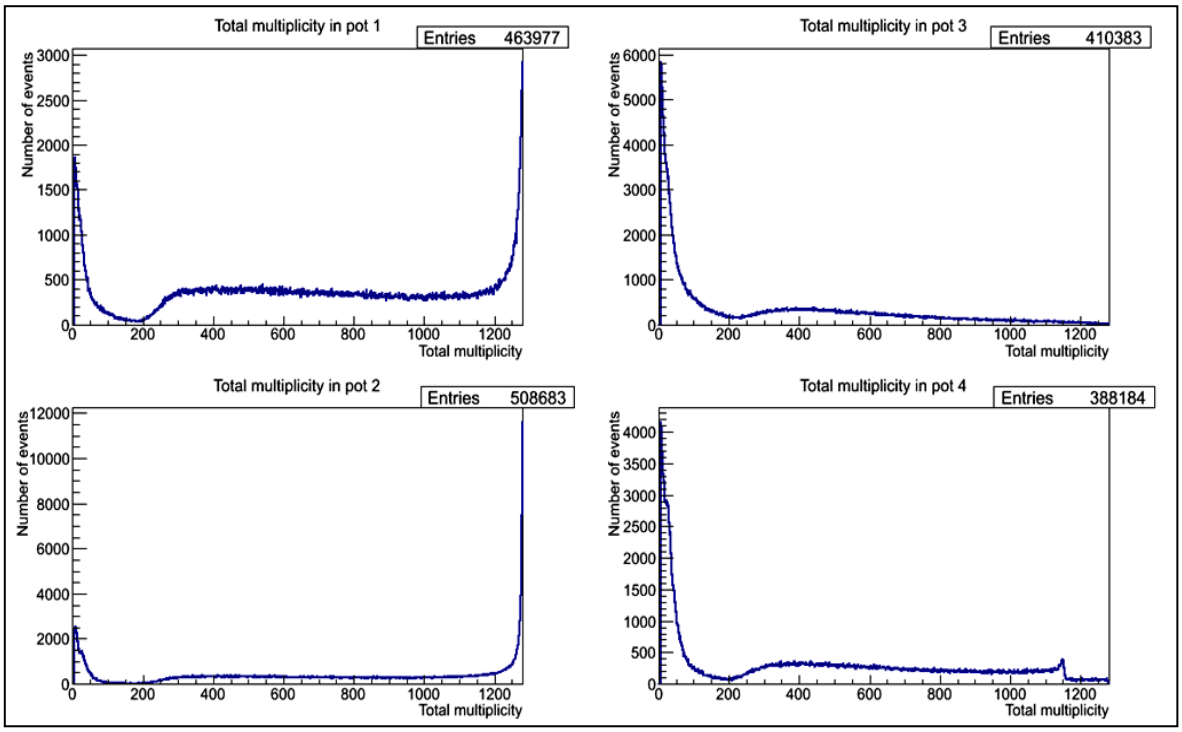

Fig.12: Total multiplicity for particular Roman Pots on A side for events without reconstructed track for nominal bunch with BCId 101.

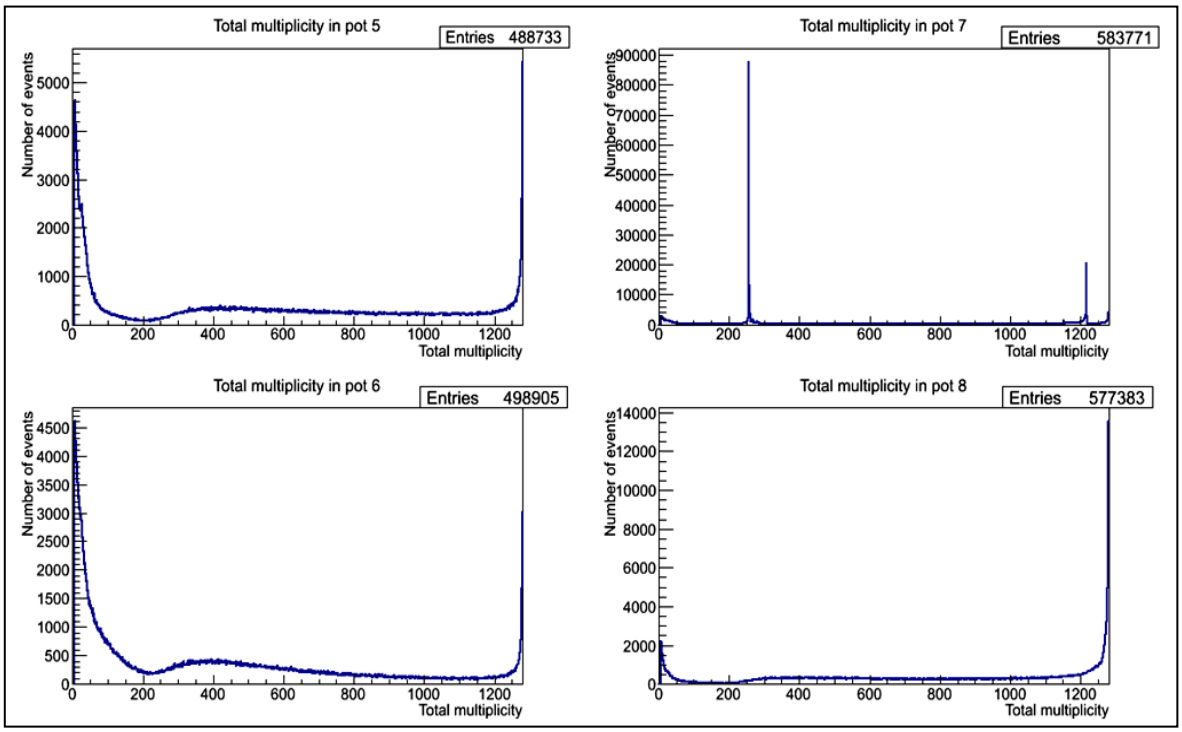

Fig.13: Total multiplicity for particular Roman Pots on C side for events without reconstructed track for nominal bunch with BCId 101.

Similarly, distributions of multiplicity in Roman Pots for BCId 1886 are presented in Fig. 14 (side A) and Fig. 15 (side C) for events without reconstruction.

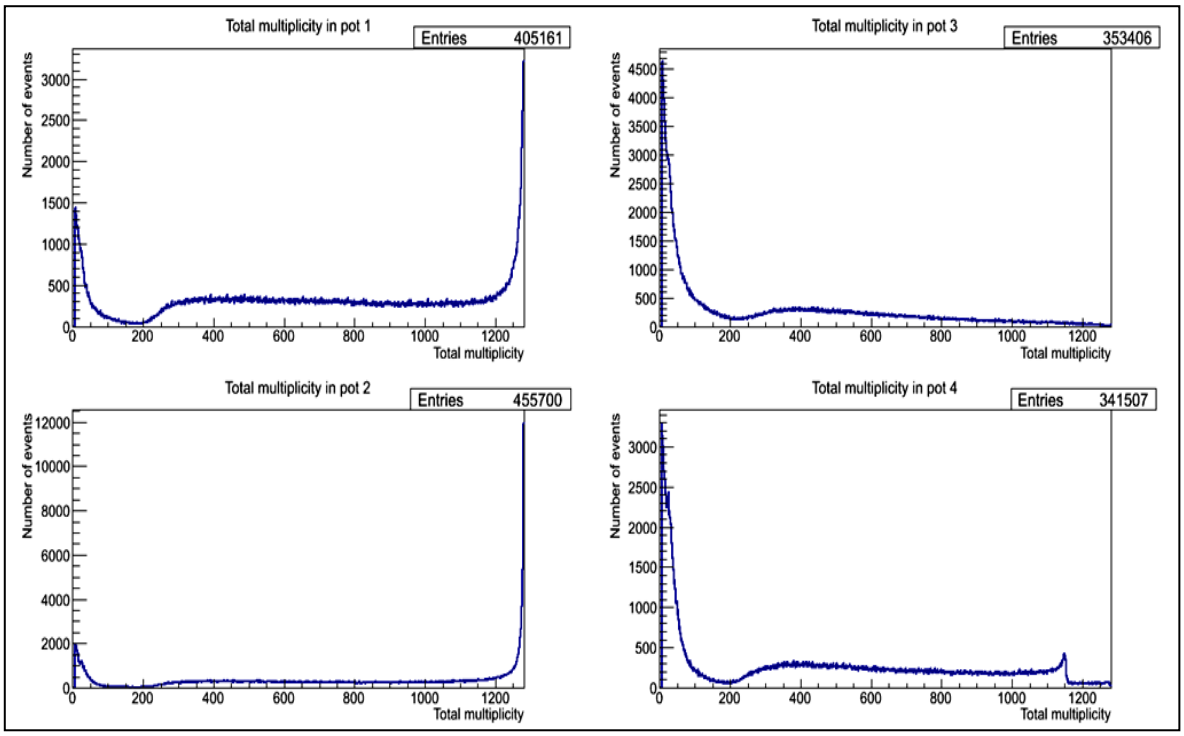

Fig.14: Total multiplicity for particular Roman Pots on A side for events without reconstructed track for nominal bunch with BCId 1886.

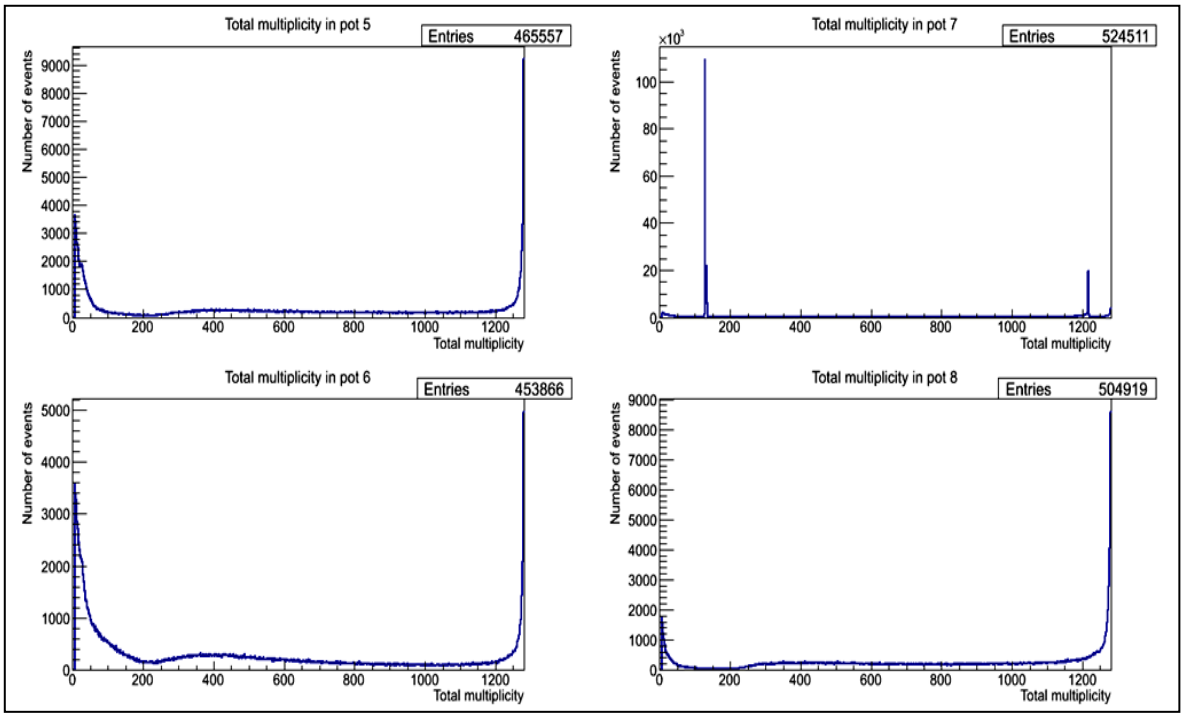

Fig.15: Total multiplicity for particular Roman Pots on C side for events without reconstructed track for nominal bunch with BCId 1886.

Histograms describing total multiplicity situation have few common aspects. First, there is lot of showers which can be observed as high peak of total multiplicity value around 1280. Next, inner stations have lower total multiplicity signalizing showers. This can be explained that particles with energy high enough can generate shower by hitting inner station. Products of this collision are detected by outer stations, which raise the statistics of total multiplicity corresponding to showers. And the last aspect, there is difference between A and C side, but not clearly to be seen, caused by different intensity of the beams. More information about this topic is presented later.

6.5.3 Layer multiplicity investigation

Investigation of total multiplicity in Roman Pots without reconstructed track has revealed known issue on Roman Pot B7R1U. Its total multiplicity is unusual for both BCId in cases where reconstruction algorithm fails. The explanation for peak around 150 for BCId 1886 (see Fig.15) and peak around 230 for BCId 101 (see Fig.13) is unknown. There is a peak around total multiplicity value 1200. This can be explained as one or two layers are not working properly. This can be shown by investigation of multiplicity in particular layer. Layer multiplicity is number describing how many times in whole run this particular layer gave a signal. It is not actually needed to know how many fibers in layer are hit in this investigation. However, we need to know if the layer gave a signal or not. Layer multiplicity investigation for both nominal bunches is presented in Fig.16 for A side and Fig.17 for C side.

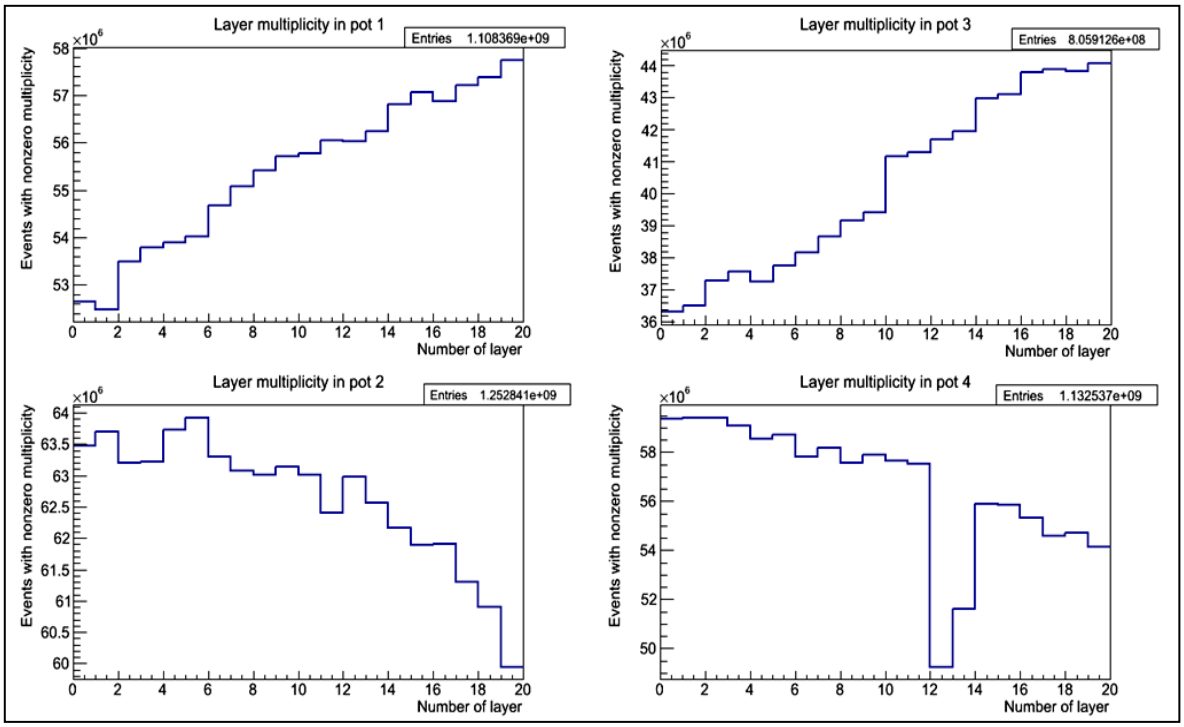

Fig.16: Layer multiplicity for particular Roman Pots on A side for both nominal bunches together.

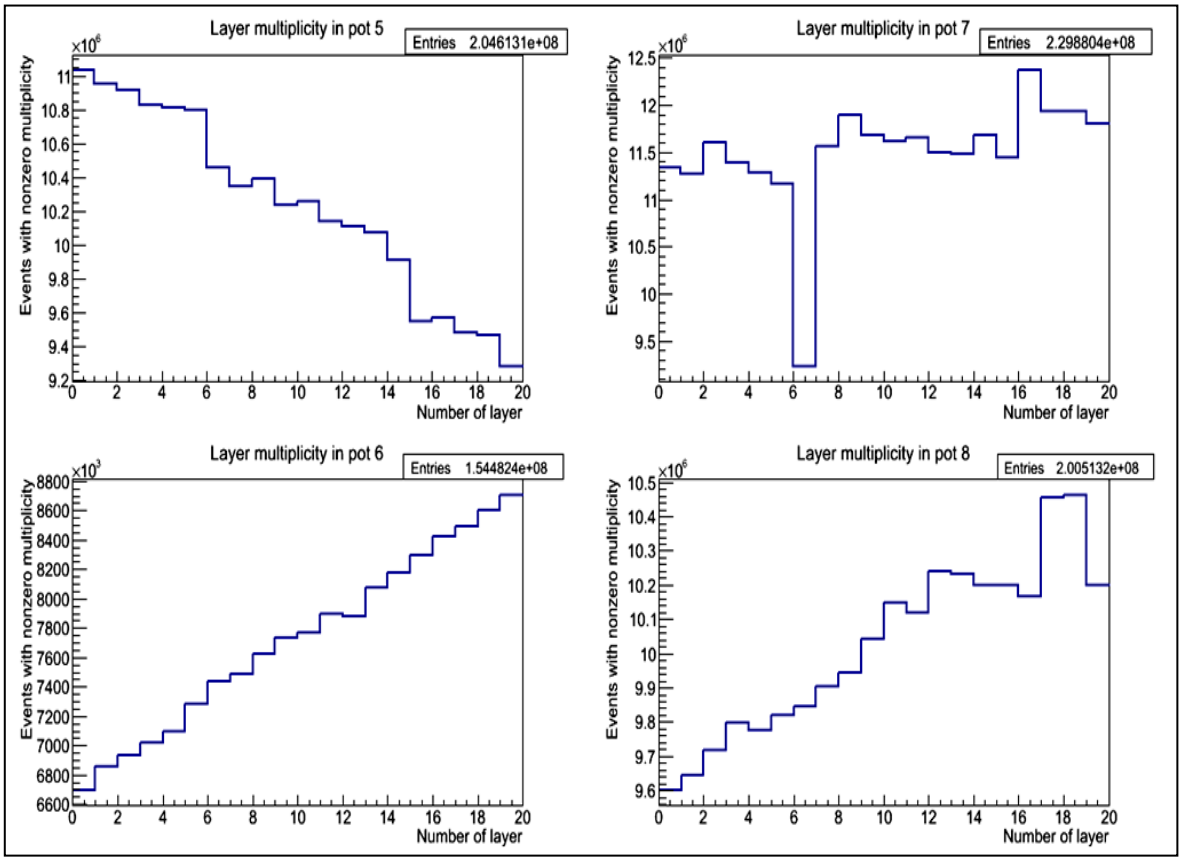

Fig.17: Layer multiplicity for particular Roman Pots on C side for both nominal bunches together.

Distributions of layer multiplicity are shown in Fig.18 (side A) and Fig. 19 (side C) for nominal bunch with BCId 101

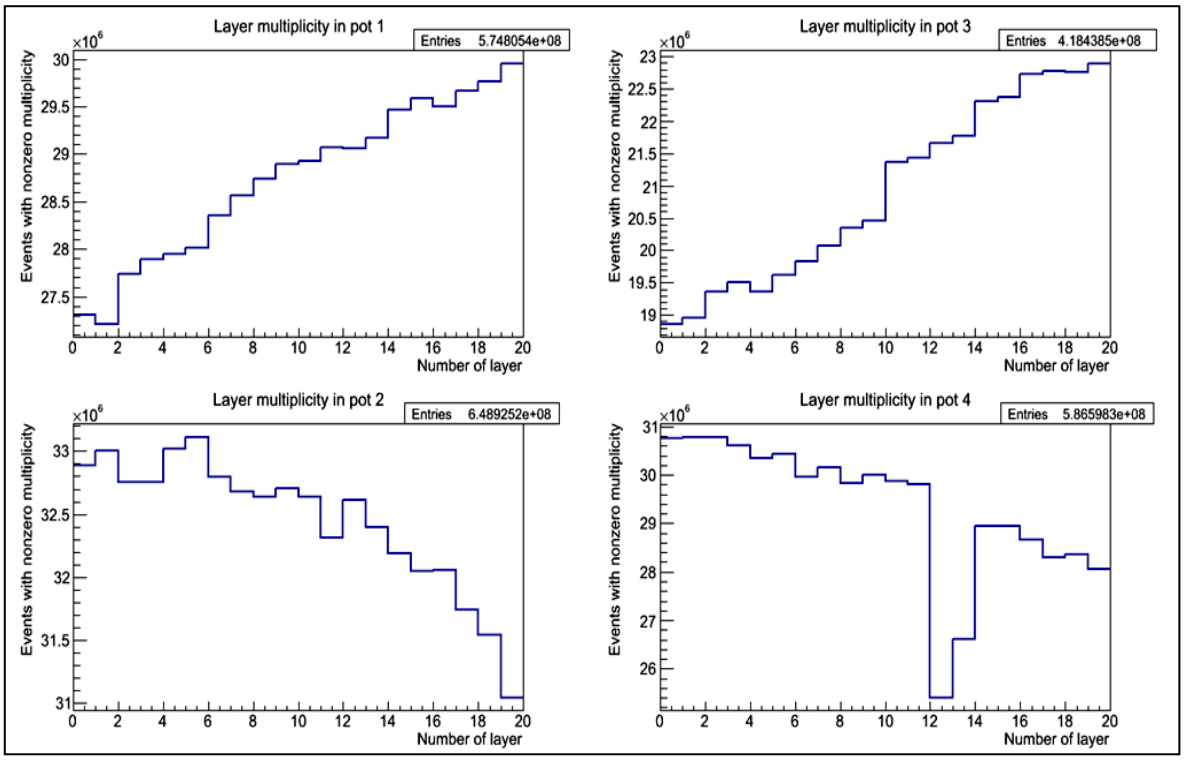

Fig.18: Layer multiplicity for particular Roman Pots on A side for nominal bunch 101.

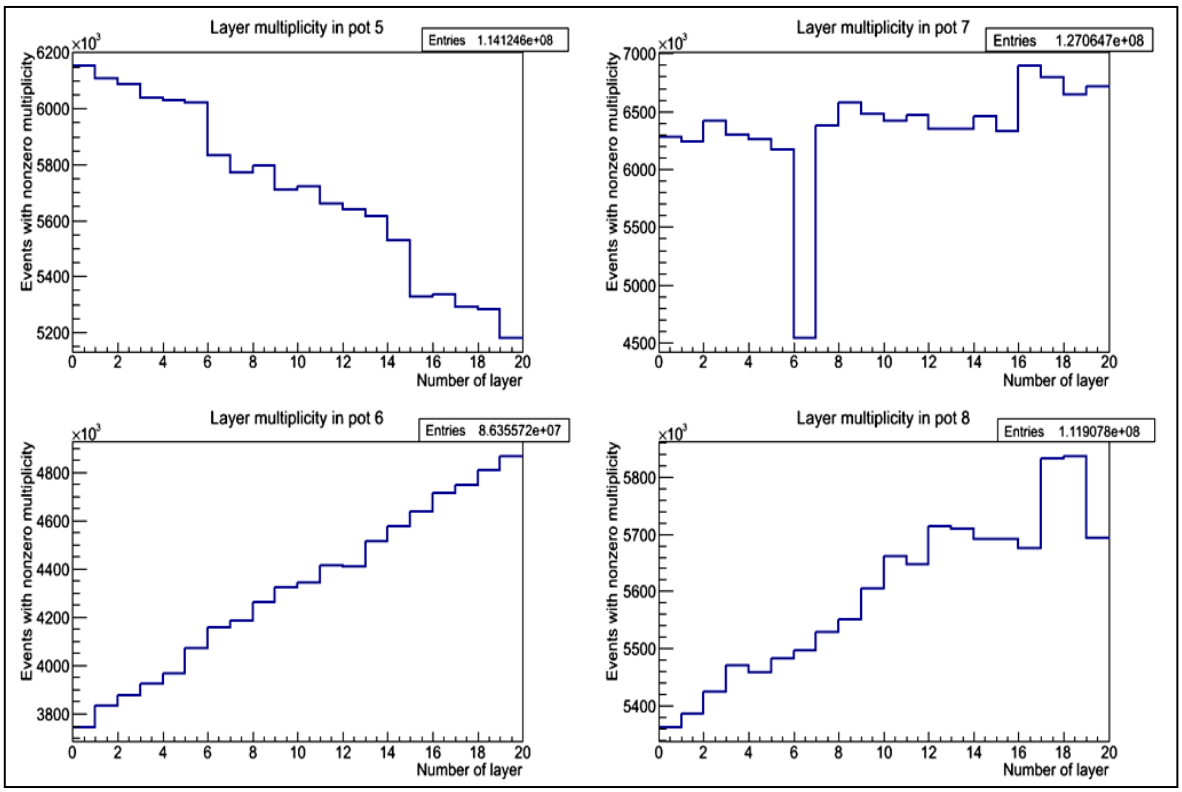

Fig.19: Layer multiplicity for particular Roman Pots on A side for nominal bunch 101.

Similarly, distributions of layer multiplicity are presented in Fig. 20 (side A) and Fig. 21 (side C) for nominal bunch with BCId 1886.

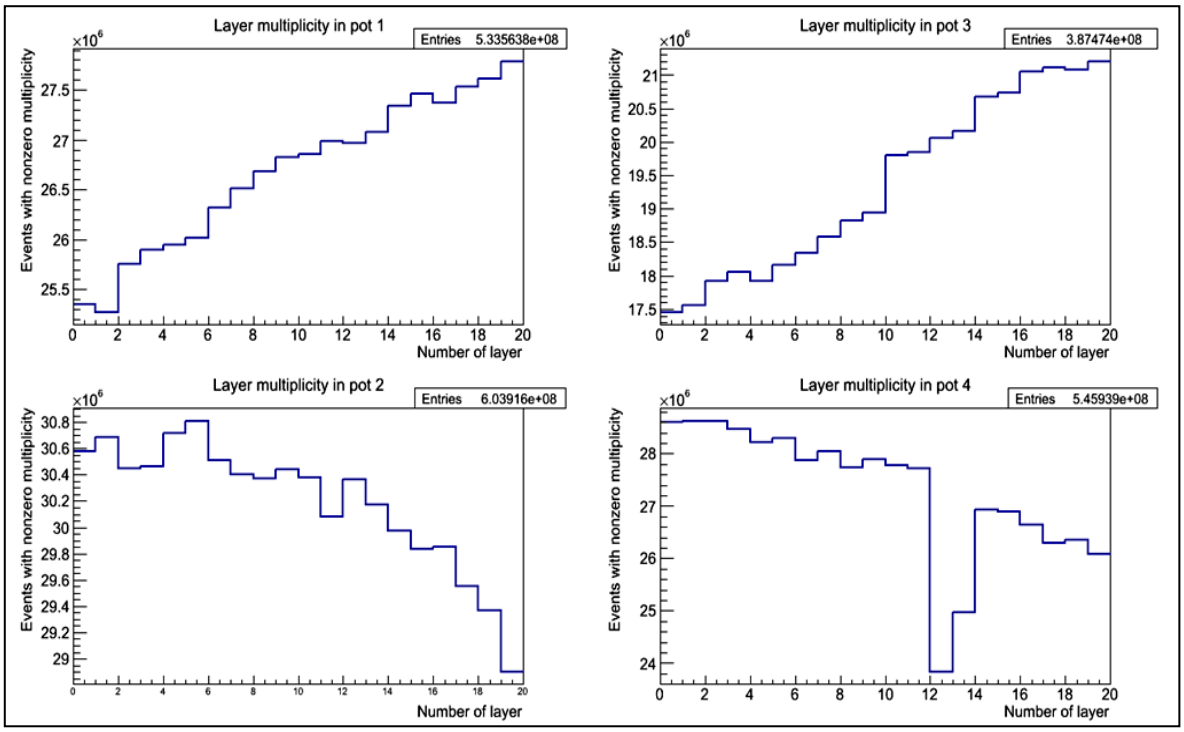

Fig.20: Layer multiplicity for particular Roman Pots on A side for nominal bunch 1886.

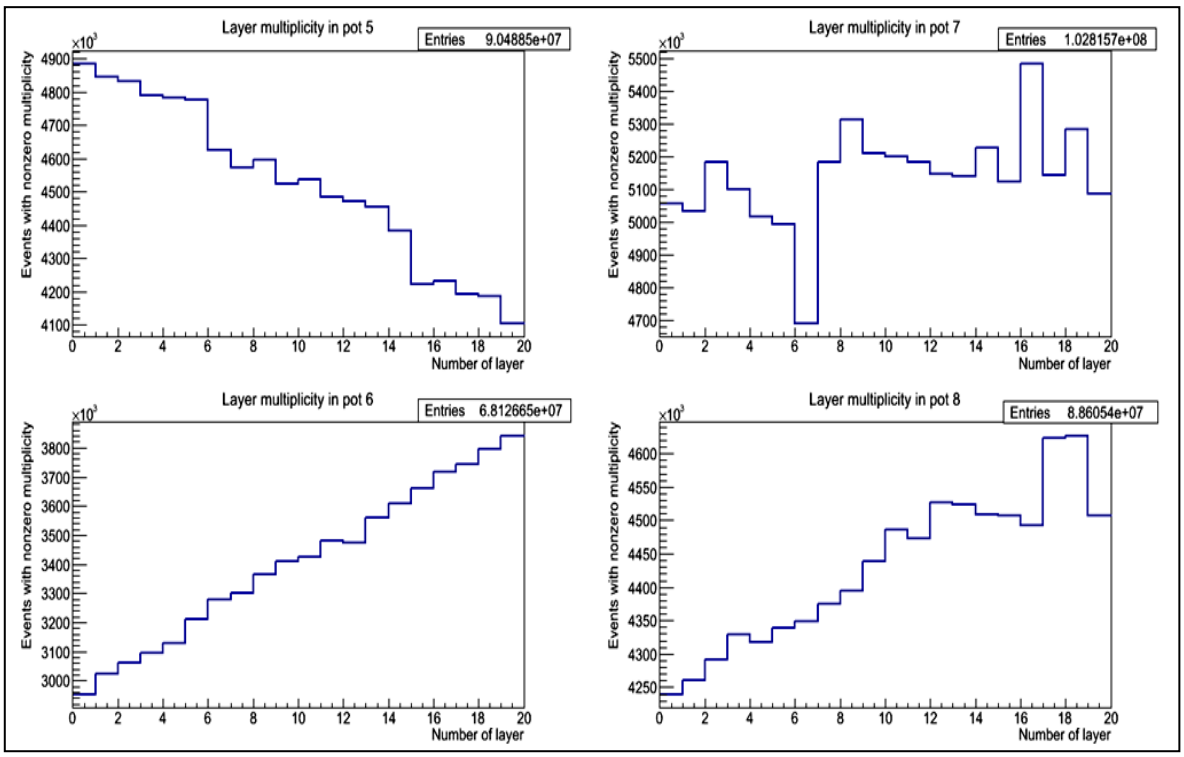

Fig.21: Layer multiplicity for particular Roman Pots on A side for nominal bunch 1886.

From all three figures above (Fig.17, Fig.19, Fig.21) is clear that 7th layer in Roman Pot B7R1U is not working properly. Its influence can be seen as a gap in corresponding histograms. On the other hand, layer multiplicity investigation reveals no explanation for other unusual peaks in Roman Pot number seven, which can be seen at Fig.11.

The statistics on both sides reveals information that layers closer to the Interaction Point have been hit les times than the layers further from Interaction Point. This points to explanation that particle hitting the first layers initiated shower generation and all other layers detected products of this shower. The layer multiplicity for lower Roman pots on A side (A7L1L and B7L1L) and upper Roman Pots on C side (A7R1U and B7R1U) shows descending statistic. This is caused by opposite position in station and layers are marked from the highest to the lowest.

Different statistic in layer multiplicity is projected to the number of reconstructed events for each Roman Pot. Reconstruction statistic is shown in Tab.13.for reconstruction events used for calculating reconstruction efficiency.

Tab.13: ***Reconstruction statistics for Roman Pots for both nominal bunches***

Roman Pot	Number of used reconstruction events	Percentage to all reconstructed events in Pot
B7L1U	658075	0.7%
B7L1L	843251	0.8%
A7L1U	763424	1.0%
A7L1L	1077943	1.0%
A7R1U	853344	5.5%
A7R1L	574442	4.9%
B7R1U	699352	5.1%
B7R1L	444911	3.1%

It is obvious that Roman Pots on side A have significantly lower reconstruction efficiency than those on side C.

This can be seen for particular nominal bunches as well. In Tab.14 there is the same statistic for nominal bunch with BCId 101.

Tab.14: ***Reconstruction statistics for Roman Pots for nominal bunche101***

Roman Pot	Number of used reconstruction events	Percentage to all reconstructed events in Pot
B7L1U	358076	0.7%
B7L1L	459551	0.8%
A7L1U	411670	1.0%
A7L1L	580050	1.0%
A7R1U	479501	5.5%

A7R1L	323148	4.9%
B7R1U	384463	5.1%
B7R1L	244670	3.1%

Statistics calculated for nominal bunch with BCId 1886 are presented in Tab.15.

Tab.15: ***Reconstruction statistics for Roman Pots for nominal bunche1886***

Roman Pot	Number of used reconstruction events	Percentage to all reconstructed events in Pot
B7L1U	299999	0.6%
B7L1L	383700	0.8%
A7L1U	351754	1.0%
A7L1L	497893	1.0%
A7R1U	373843	5.5%
A7R1L	251294	4.9%
B7R1U	314889	5.1%
B7R1L	200241	3.7%

Lower statistics for Roman Pots on A side can be explained by different beam intensity. The beam with higher intensity has more protons in bunches and there are more products following the previous course after collision measured in ALFA detectors. Intensity of Beam 1 is illustrated in Fig.22. There is time evolution of beam intensity for bunches with BCId 1 in the Fig.22 as well. Bunches with BCId 1 are pilot bunches because of their low intensity. These bunches with BCId 1 can serve as reference of intensities of pilot bunches. Intensity situation for Beam 2 is illustrated in Fig.23.

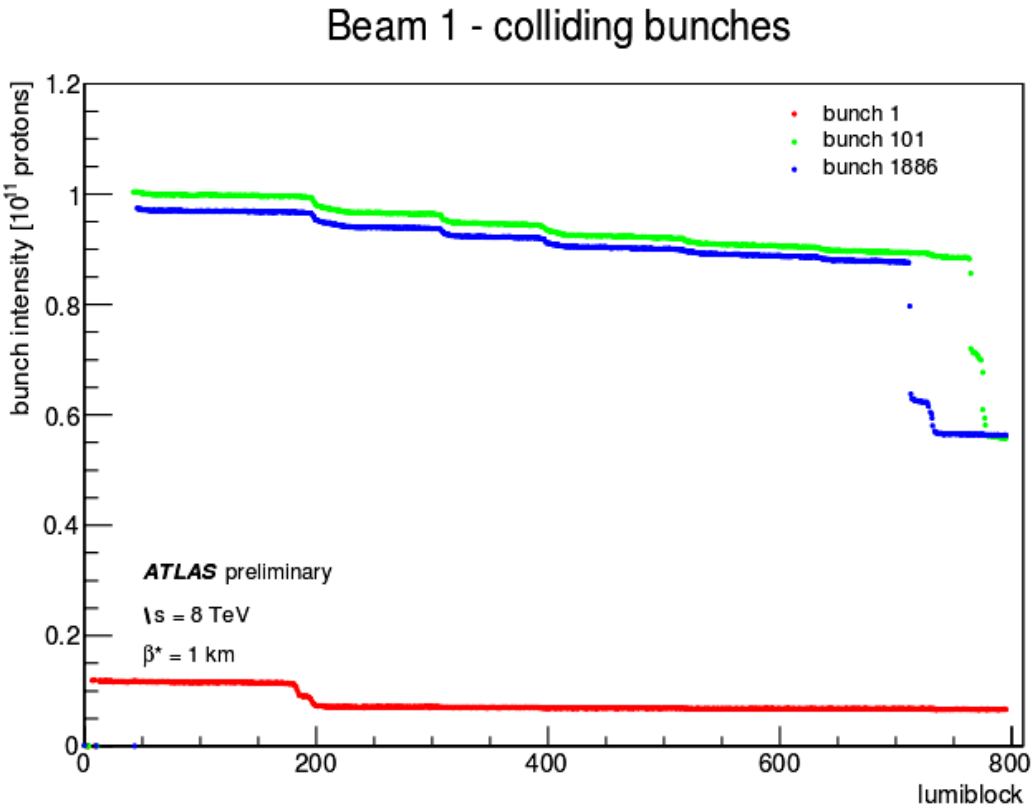

Fig.22: Evolution of beam 1 intensity over time (this picture is from Mgr. Petr Hamal).

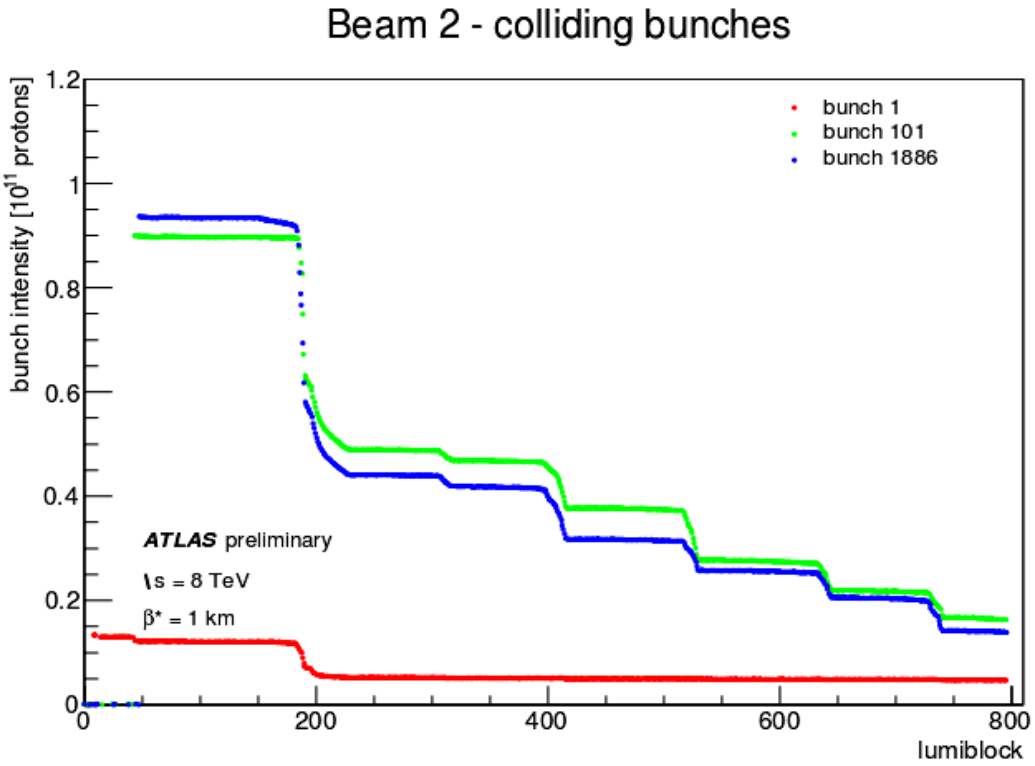

Fig.23: Evolution of beam 2 intensity over time (this picture is from Mgr. Petr Hamal).

Intensity of Beam 2 dropped around lumiblock number 200. This can explain differences of reconstruction percentage between A and C Direction of the Beam 1 and Beam 2 is shown on Fig.3. The higher shower intensity on side C is caused by higher intensity of Beam 1.

6.6 Summary for reconstruction efficiency

Reconstruction efficiency script processed Ntuple with data from run 213268. Reconstruction efficiency has been stated as 17%. Reconstruction efficiency for arm 1368 is lower than the one in arm 2457 in all BCId cases. The value of reconstruction efficiency does not meet the expectations which were around 70-80%. Further investigation revealed that script does not give wrong numbers. Multiplicity investigation revealed high presence of showers. The difference of intensities between B 1 and Beam 2 caused different statistic of layer multiplicity between A side and C side. This affects rate of successful reconstruction in each Roman Pot.

7. Reconstruction of spectrum of Mandelstam variable *t*

7.1 Introduction

Ntuple with data for reconstruction of spectrum of Mandelstam variable *t* has been processed by script named Mandel.C. This script is added on the attached CD, which is part of this thesis.

7.2 Effective optics

Effective optics used for calculation of the spectrum has been imported from simulation file. Effective optics is presented in Tab.16.

Tab.16: ***Effective optics used for calculation of*** **t** ***spectrum***

Energy of the beam	4000 GeV
Distance between station 1 and 2	4149.0 mm
Distance between station 3 and 4	4143.8 mm
Beam 1 $\beta_x^\star$	1000.00891 m
Beam 1 $\alpha_x^\star$	-0.00299998
Beam 1 $\beta_y^\star$	1000.008929 m
Beam 1 $\alpha_y^\star$	-0.00299996
Beam 2 $\beta_x^\star$	100.008929 m
Beam 2 $\alpha_x^\star$	-0.00300001
Beam 2 $\beta_y^\star$	1000.009031 m
Beam 2 $\alpha_y^\star$	-0.00299997
Station B7L1 β_x	256.0663358 m
Station B7L1 α_x	3.51121684
Station B7L1 β_y	99.67813224 m
Station B7L1 α_y	0.40784752
Station B7L1 Ψ_x	0.5002995154 rad
Station B7L1 Ψ_y	0.2524401642 rad
Station A7L1 β_x	286.031353 m
Station A7L1 α_x	3.72671017
Station A7L1 β_y	103.255661 m
Station A7L1 α_y	0.45628990
Station A7L1 Ψ_x	0.4977947655 rad
Station A7L1 Ψ_y	0.2459435930 rad
Station A7R1 β_x	289.315942 m
Station A7R1 α_x	3.72705669
Station A7R1 β_y	103.369676 m
Station A7R1 α_y	0.439626328
Station A7R1 Ψ_x	0.4977203883 rad
Station A7R1 Ψ_y	0.2459498970 rad

Station B7R1 β_x	259.338010 m
Station B7R1 α_x	3.513972888
Station B7R1 β_y	99.9274245 m
Station B7R1 α_y	0.456289901
Station B7R1 Ψ_x	0.500125957 rad
Station B7R1 Ψ_y	0.252434774 rad

These values are needed to calculate particular lever arms and transport matrix elements as it is described in Chapter 3.

7.3 Distribution of hit signals in Roman Pots

The edge cut is the only filter used on sample for studying elastic sample. Distribution of hits in particular Roman Pots is illustrated in Fig.24 for A side and situation on C side is shown on Fig.25.

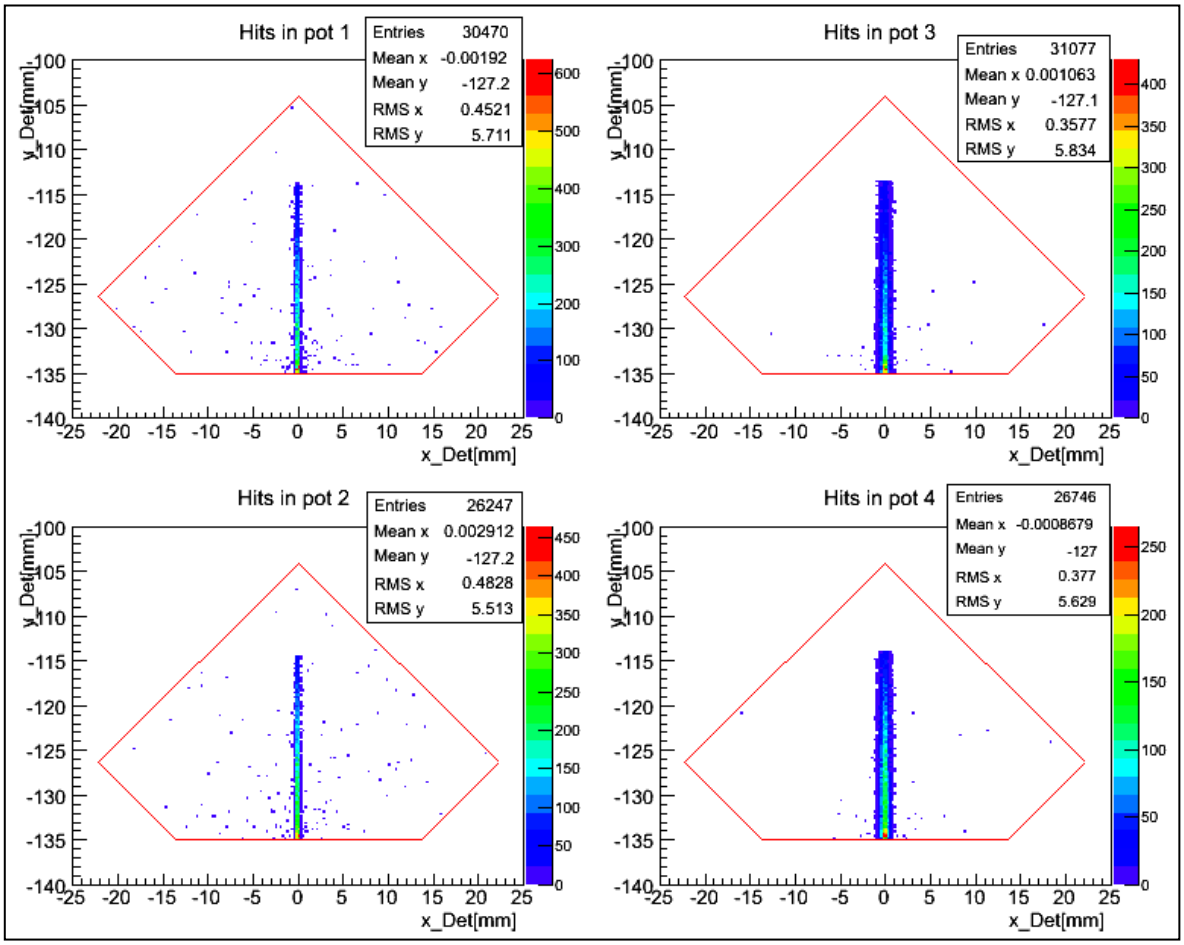

Fig.24: Hit distribution in particular Roman Pots on A side.

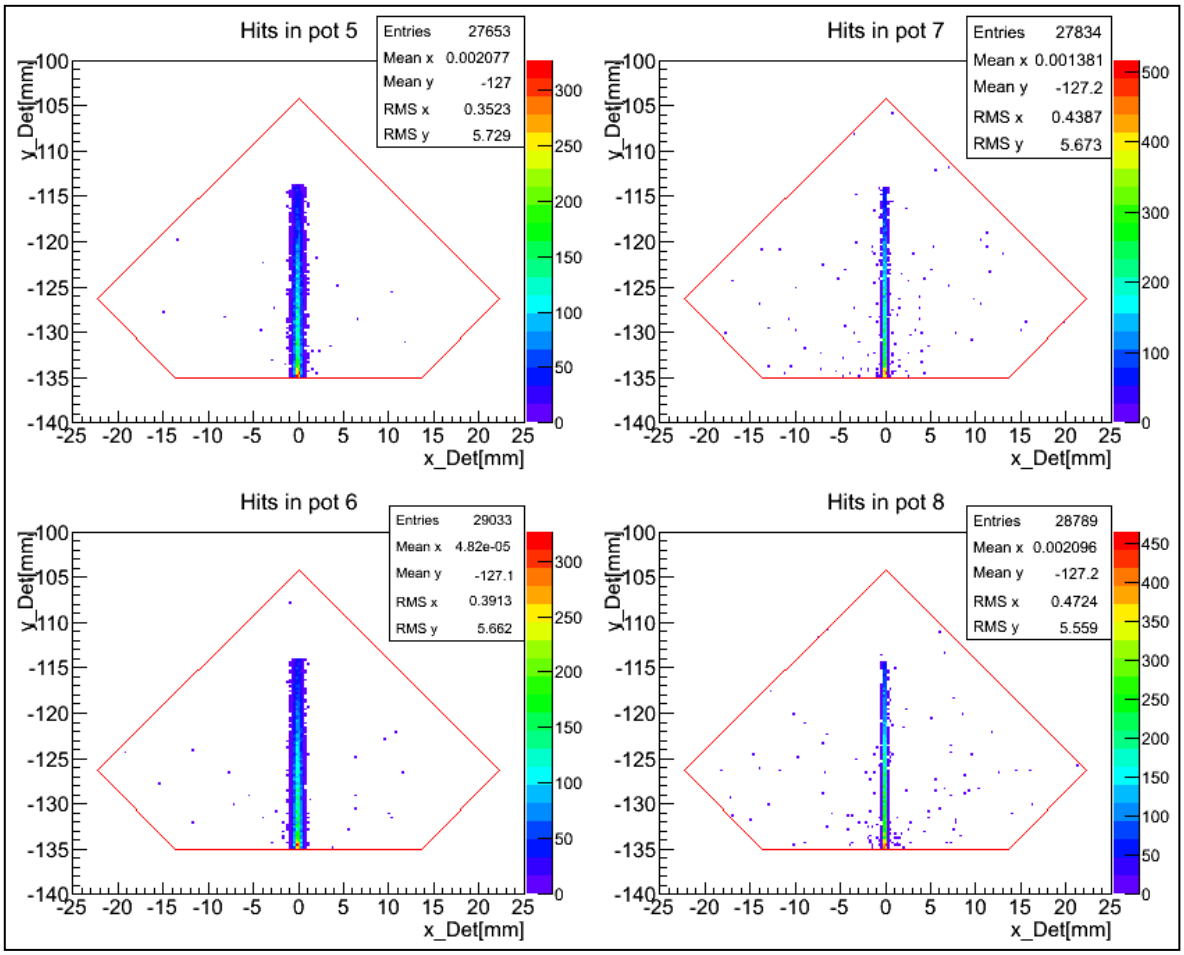

Fig.25: Hit distribution in particular Roman Pots on C side.

Red lines illustrate the shape of the detector. The spot left by products of beam have elliptic shape oriented in vertical axis. Spots in Roman Pots B7L1U and B7L1L on Fig.24 (signed as 1 and 2) belong together. In Roman Pot B7L1U, there is upper half of elliptic spot and the lower part is in B7L1L.. Events in space between these halves have been filtered out by edge cut. There are more tracks reconstructed in outer stations outside the elliptic spot. Simulations indicate generation of showers in inner ALFA detectors. Outer stations detect products of these showers.

7.4 Reconstruction of Mandelstam variable *t*

7.4.1 General information

Reconstruction of Mandelstam variable *t* can be made by several methods using measured positions of hits in detectors and knowledge of effective optics. These methods are described in the Chapter 3. Calculation of reconstruction of Mandelstam variable *t*

always use scattering angle. Distribution of scattering angle and *t* spectrum is shown For each method.

7.4.2 Subtraction method

Subtraction method is the primary method used on ALFA detectors. Fig.26 illustrates the distributions of scattering angle for both arms and for horizontal and vertical axes.

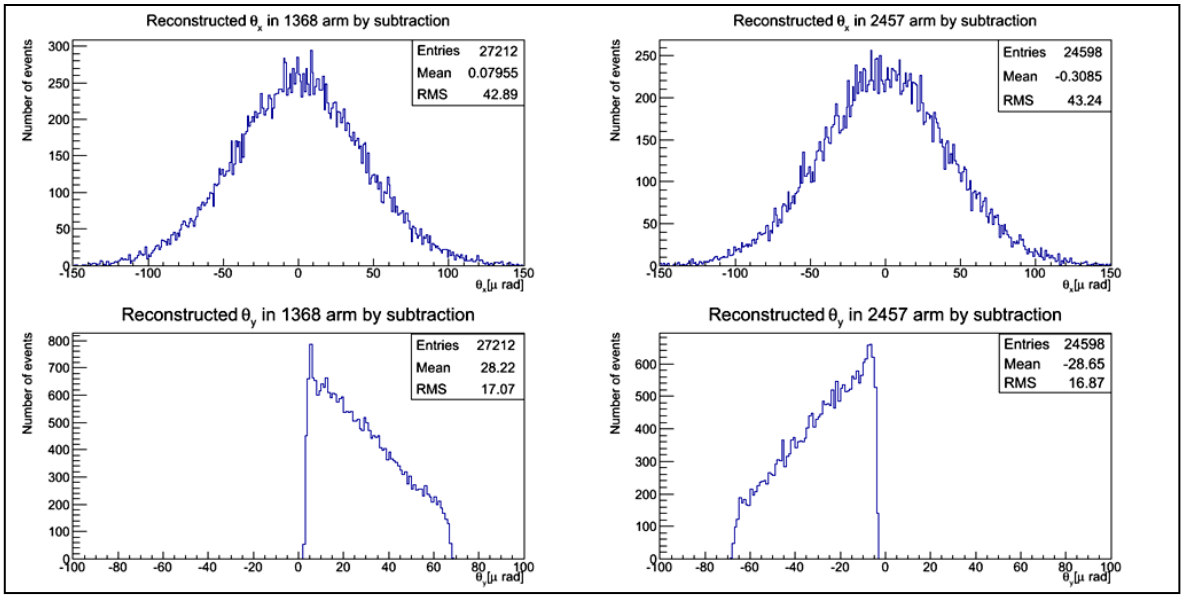

Fig.26: Histograms of reconstructed scattering angles for both arms and horizontal and vertical axis by subtraction method.

Reconstructed values of Mandelstam variable *t* by subtraction method are illustrated in Fig. 27.

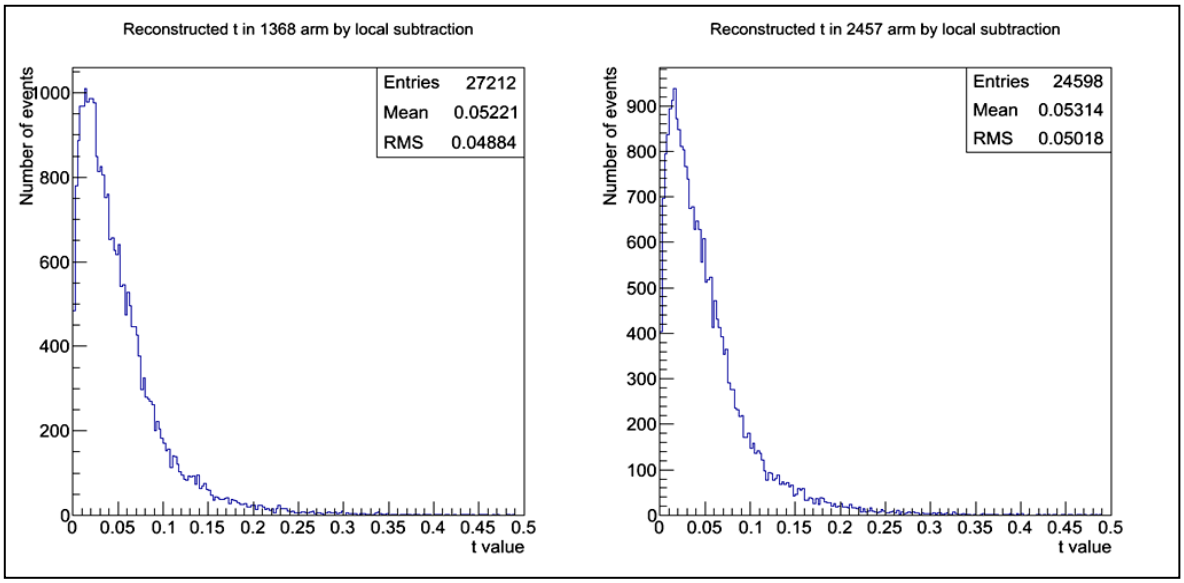

Fig.27: Reconstructed values of Mandelstam variable *t* in both arms by subtraction method.

It is obvious that Mandelstam variable *t* values varies around zero. The zero value corresponds to event, where the particle travels after collision without change of direction. These events are not important for analysis because they miss the area of the detector. The subtraction method is the most precise from all four presented. One reason is that it gives lower statistics for zero value of Mandelstam variable *t*.

7.4.3 Local angle method

Theta reconstruction for local angle method is presented in Fig.28 for both arms and for horizontal and vertical axes.

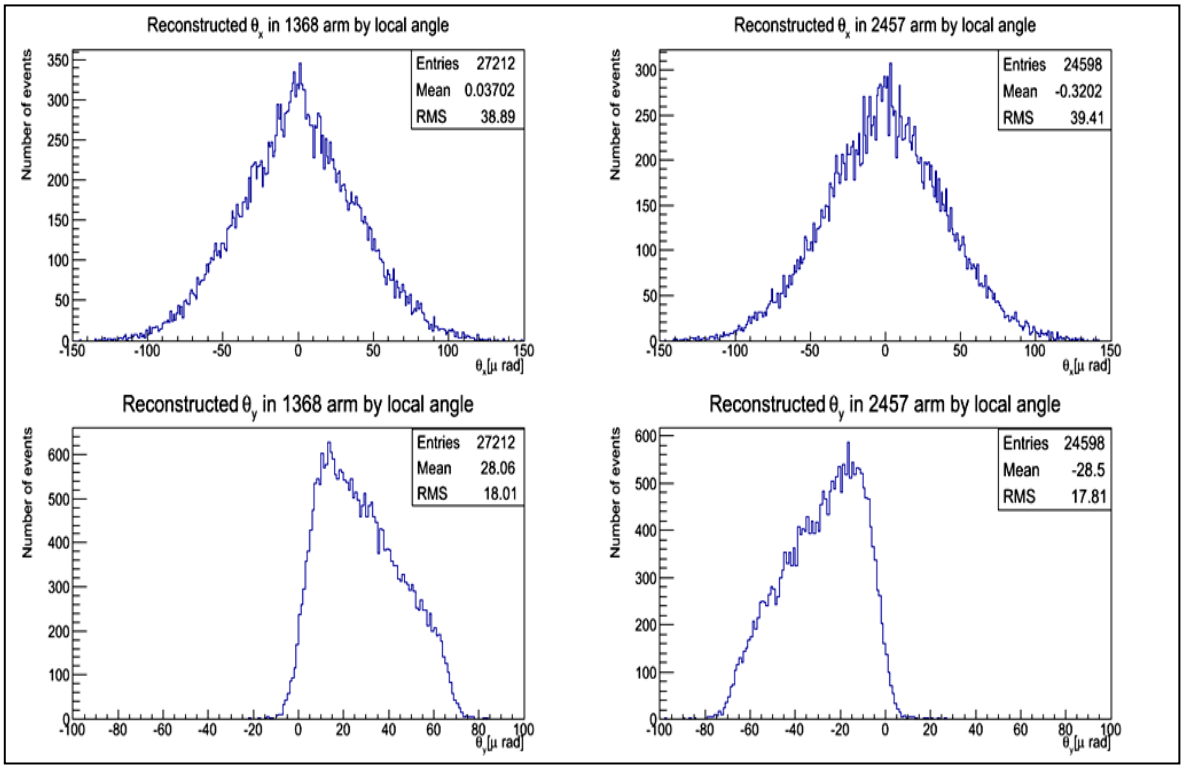

Fig.28: Histograms of reconstructed scattering angles for both arms and horizontal and vertical axis by local angle method.

Reconstructed values of Mandelstam variable *t* by local angle method are shown in Fig.29 for both arms.

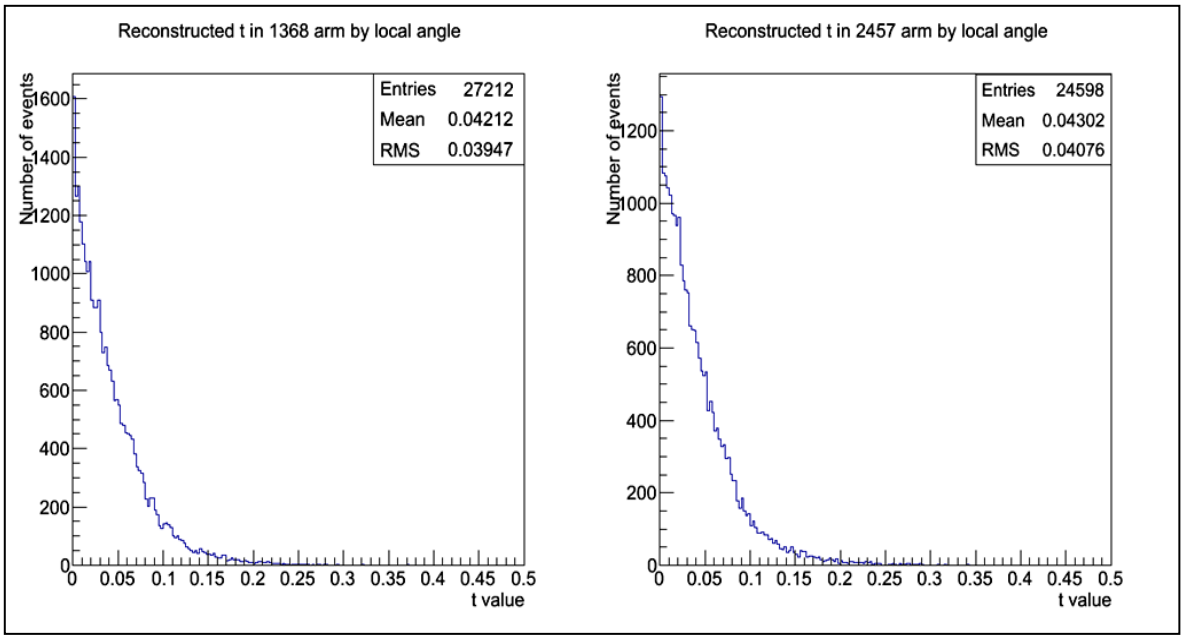

Fig.29: Reconstructed values of Mandelstam variable *t* in both arms by local angle method.

We can see that reconstruction of Mandelstam variable *t* by local angle is not as precise as in the subtraction method. This is obvious from comparison of values around zero.

7.4.4 Local subtraction method

Reconstructed values of scattering angle for both arms and horizontal and vertical axes are presented in Fig.30.

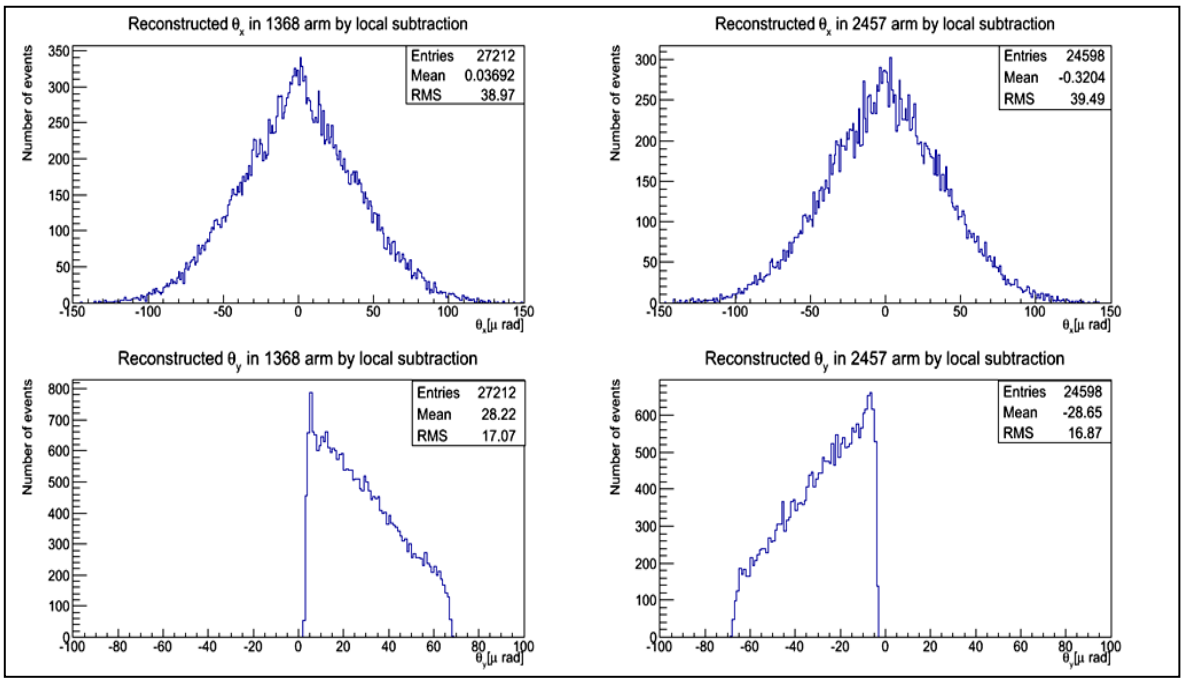

Fig. 30: Histograms of reconstructed scattering angles for both arms and horizontal and vertical axis by local subtraction method.

Reconstructed values of Mandelstam variable *t* by local subtraction method are shown in Fig.31 for both arms.

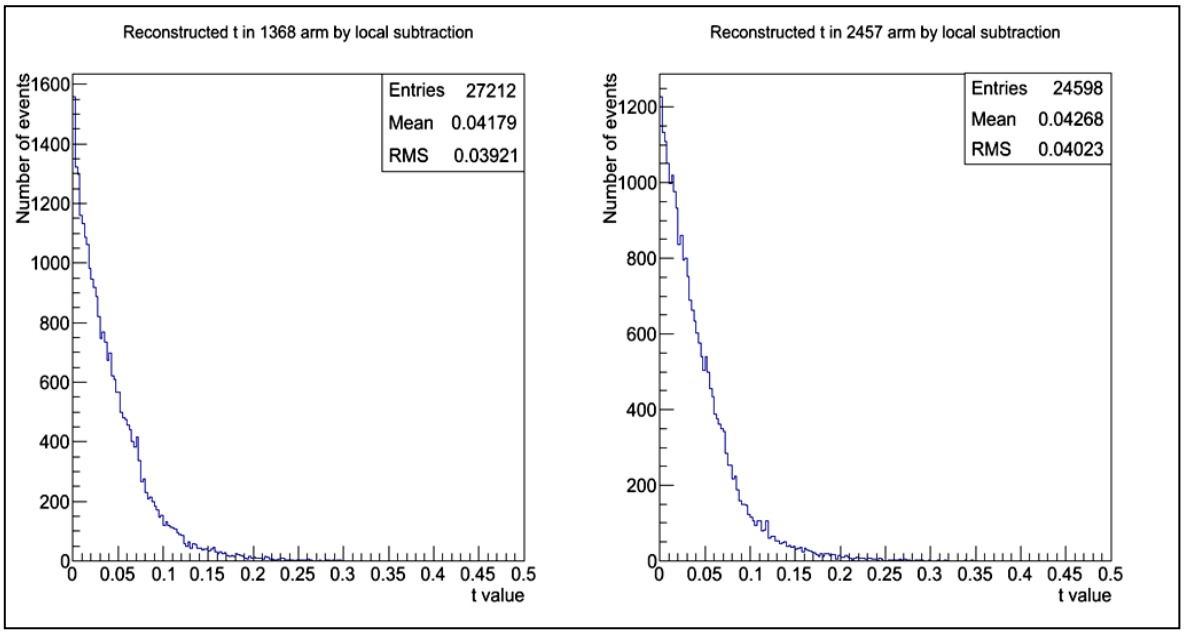

Fig.31: Reconstructed values of Mandelstam variable *t* in both arms by local subtraction method.

Again the precision of reconstruction process is again worse compared with the subtraction method.

7.4.5 Lattice method

Reconstructed values of scattering angle for both arms and horizontal and vertical axes are illustrated in Fig.32.

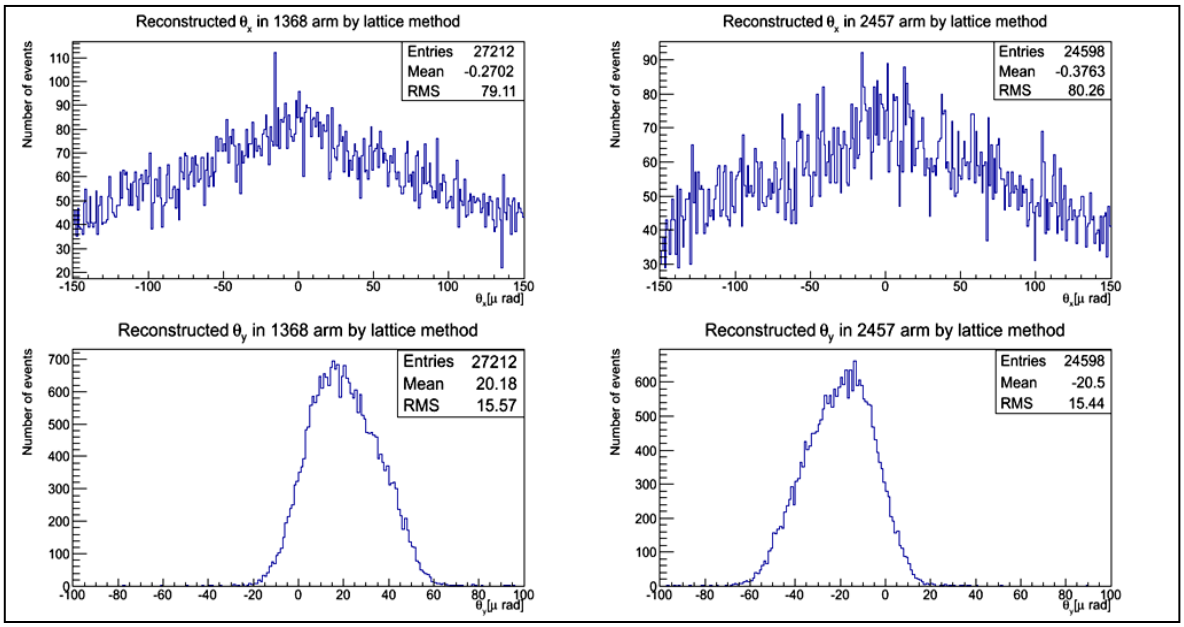

Fig.32: Histograms of reconstructed scattering angles for both arms and horizontal and vertical axis by lattice method.

Reconstructed values of Mandelstam variable *t* by lattice method are shown in Fig.33 for both arms.

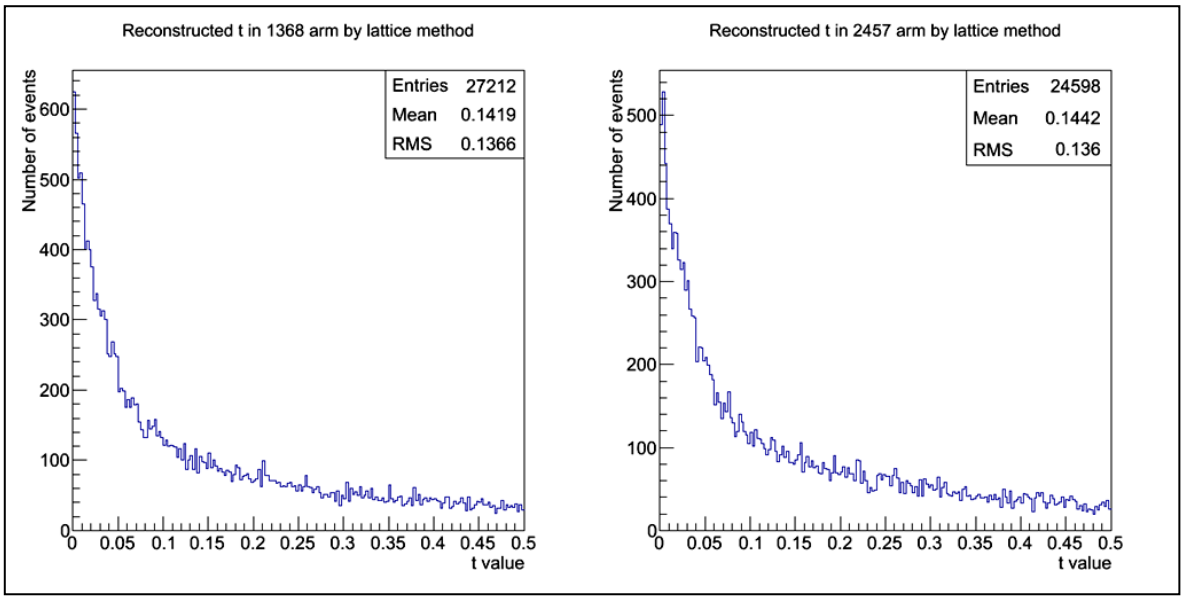

Fig.33: Reconstructed values of Mandelstam variable *t* in both arms by lattice method.

The lattice method gives the worst distributions of scattering angle (see Fig.32) as well as the worst distributions for Mandelstam variable *t* (see Fig.33).

7.5 Summary for reconstruction of Mandelstam variable *t*

As it was expected, we get the best results of reconstruction of Mandelstam variable *t* are from the subtraction. The worst results are obtained from the lattice method. Results from local angle and local subtraction methods are similar in all distributions (see Fig.28-31).

Distributions of reconstruction of scattering angles are similar for subtraction, local angle and local subtraction methods (see Fig.26, Fig.28 and Fig.30). Only the lattice method distribution is not corresponding well to other methods (see Fig.32).

Summary

Nowadays, the Large Hadron Collider is one of the best tools for study of major tasks in particle physics domain. Data collected during year 2012 has revealed presence of Higgs boson and confirmed another part of Standard Model.

First analysis of data from run 213268 is outcome of this work. Analysis of this run is not yet complete because there is a lot of problems which are not yet well understood. Analysis in this work focused on evaluation of reconstruction efficiency for run 213268, which is basic analysis and it can be made on raw data. The reconstruction efficiency was calculated but the results are not corresponding to first expectations. The second task of this work was to illustrate expectations for reconstruction of Mandelstam variable *t* for several calculation methods. This task was done on a simulation sample with elastic events only. Both tasks were made by studying products of proton-proton collisions in the ALFA detector.

The reconstruction efficiency for run 213268 is 17%. Its low value of is caused by presence of showers. This was proved by investigation of multiplicity. Reconstruction efficiencies for particular arms vary slightly but this was expected. Analysis of reconstruction of Mandelstam variable *t* proved that subtraction method gave best results. Methods of local angle and local subtraction gave comparable results but not as precise as subtraction method. The lattice method gave worst results.

List of sources

[1] CERN contributors: *The large hadron collider*, [online], CERN, c2014 [quoted 3.6.2014] http://home.web.cern.ch/topics/large-hadron-collider

[2] Jakobsen, S.: *Commissioning of the Absolute Luminosity For Atlas detector at the LHC*, [online] PhD Thesis, The Faculty of Science University of Copenhagen 2013, [quoted 3.6.2014] https://cds.cern.ch/record/1637195/files/CERN-THESIS-2013-230.pdf

[3] Wikipedia contributors: *Large hadron collider*, [online], Wikipedia: The Free Encyclopedia, c2014, [quoted 3.6.2014] http://en.wikipedia.org/wiki/Large_Hadron_Collider

[4] CERN contributors *ATLAS experiment*, [online], CERN, c2014 [quoted 9.6.2014] http://www.atlas.ch/photos/index.html

[5] Wikipedia contributors: *ATLAS Experiment*, [online], Wikipedia: The Free Encyclopedia, c2014, [quoted 3.6.2014] http://en.wikipedia.org/wiki/ATLAS_experiment

[6] Stenzel, H.: *The ATLAS Experiment*,[online], CERN c2011 [quoted 3.6.2014] http://atlas-project-lumi-fphys.web.cern.ch/atlas-project-lumi-fphys/ALFA/default.html

[7] ATLAS Collaboration, *Measurement of the total cross section in* pp *collisions at* $\sqrt{s} = 7$ *TeV from elastic scattering with the ATLAS detector.* ATLAS note**,** 2013

[8] Muirhead, H., *The physics of elementary particles*, Pergamon press, Oxford, Great Britain, 1965

[9] ATLAS Collaboration, *ATLAS Forward Detectors for Measurement of Elastic Scattering and Luminosity.* ATLAS note, 2008

[10] ROOT Collaboration, *ROOT Data Analysis Framework*, [online], User´s Guide, 2014 [quoted 30.6.2014] http://root.cern.ch/root/htmldoc/guides/users-guide/ROOTUsersGuideA4.pdf

[11] CERN contributors to *ATLAS Roman Pots* [online], CERN, c2014 [quoted 28.6.2014] https://twiki.cern.ch/twiki/bin/view/Atlas/AtlasRomanPots

Appendix

Analysis of reconstruction efficiency was made by means of script named *RecoEff.C*, which is on attached CD in the folder *scripts/RecoEff*. This script for calculation of reconstruction efficiency takes into account information about lumiblocks time and energy. This information is stored in the file *LumiTimeEnergy.dat*. It can be found in the *scripts/RecoEff* folder as well. Figures and outputs from the script used in this work for reconstruction efficiency are in folder *outputs/RecoEff/* where they are sorted by BCId. For example, output path for BCId 101 is *outputs/RecoEff/B101/*. Figures for both BCIds and for the whole run are stored in *outputs/RecoEff/General*.

A script for reconstruction of Mandelstam variable *t* is named *Mandel.C* and it can be found on CD in the folder *scripts/Mandel/*. Figures from the script used in work are saved in the folder *outputs/Mandel/* where they are sorted by used method of reconstruction. For example, output directory for the subtraction method is *outputs/Mandel/Subtraction/*. Hitmaps are saved in the folder *outputs/Mandel/Hitmaps/*.